AN EXPERIMENTAL METHOD FOR DETERMINING HEAT TRANSFER DISTRIBUTIONS ON BLUNT BODIES AT HYPERSONIC MACH NUMBERS

Frederick Karl Hube

ARO, Inc.

June 1969

VON KÁRMÁN GAS DYNAMICS FACILITY
ARNOLD ENGINEERING DEVELOPMENT CENTER
AIR FORCE SYSTEMS COMMAND
ARNOLD AIR FORCE STATION, TENNESSEE

NOTICES

When U. S. Government drawings specifications, or other data are used for any purpose other than a definitely related Government procurement operation, the Government thereby incurs no responsibility nor any obligation whatsoever, and the fact that the Government may have formulated, furnished, or in any way supplied the said drawings, specifications, or other data, is not to be regarded by implication or otherwise, or in any manner licensing the holder or any other person or corporation, or conveying any rights or permission to manufacture, use, or sell any patented invention that may in any way be related thereto.

Qualified users may obtain copies of this report from the Defense Documentation Center.

References to named commercial products in this report are not to be considered in any sense as an endorsement of the product by the United States Air Force or the Government.

AN EXPERIMENTAL METHOD FOR DETERMINING HEAT TRANSFER DISTRIBUTIONS ON BLUNT BODIES AT HYPERSONIC MACH NUMBERS

Frederick Karl Hube
ARO, Inc.

FOREWORD

The work reported herein was sponsored by the Arnold Engineering Development Center (AEDC), Air Force Systems Command (AFSC), under Program Element 65401F/876A.

The results of research presented were obtained by ARO, Inc. (a subsidiary of Sverdrup & Parcel and Associates, Inc.), contract operator of AEDC, AFSC, Arnold Air Force Station, Tennessee, under Contract F40600-69-C-0001. The work was conducted over the period from December 1966 to January 1968 under ARO Project Numbers VT2715, VT0878, and VT2914. The manuscript was submitted for publication on December 16, 1968.

The author wishes to acknowledge the personnel in the von Kármán Gas Dynamics Facility (VKF), Arnold Engineering Development Center, whose assistance was invaluable during the preparation of this study. The author is indebted to Mr. J. C. Sivells, Mr. H. W. Ball, and Mr. L. L. Trimmer of ARO, Inc. for their suggestions and assistance. Thanks are also due Mr. R. L. Ledford and Mr. C. T. Kidd for their preparation of the calorimeters and heat gages reported herein, and to Mr. R. K. Matthews and Mr. R. H. Eaves for their skin heat transfer data. The author is particularly grateful to Dr. F. Shahrokhi of the University of Tennessee Space Institute for his guidance during the preparation of this material.

This technical report has been reviewed and is approved.

Eugene C. Fletcher
Lt Colonel, USAF
AF Representative, VKF
Directorate of Test

Roy R. Croy
Colonel, USAF
Director of Test

ABSTRACT

Experimental convective heat transfer distributions on a hemisphere-cylinder configuration were obtained using slug calorimeters and Gardon gages. Wind tunnel tests were conducted at a nominal Mach number of 10 over a free-stream Reynolds number range from 0.31×10^6 to 1.04×10^6 based on the model diameter (5.80 inches). The data were compared with theoretical heat transfer values and data obtained with thin-skin calorimetric wind tunnel models.

The slug calorimeter data were highly time dependent due to conduction heat losses; consequently, the data did not compare favorably with theoretical predictions. Gardon gage indicated heat transfer was in very good agreement with both theoretical values and data from other sources.

TABLE OF CONTENTS

CHAPTER		PAGE
I.	INTRODUCTION	1
II.	APPARATUS	4
	Wind Tunnel	4
	Model	6
	Calorimeters	6
	Slug calorimeters	6
	Gardon gages	11
	Instrumentation	11
III.	CALORIMETER THEORY	14
	Slug Calorimeter	14
	Gardon Gage	21
IV.	PROCEDURE	26
	Test Procedures	26
	Data Reduction	26
	Slug Calorimeter and Gardon Gage Calibration	29
	Slug calorimeters	29
	Gardon gages	29
	Data Precision	31
V.	RESULTS AND DISCUSSION	33
	Slug Calorimeter Results	33
	Gardon Gage Results	40
VI.	CONCLUSIONS	47

CHAPTER PAGE

BIBLIOGRAPHY 49

APPENDIX 53

LIST OF TABLES

TABLE		PAGE
I.	Slug Calorimeter Locations and Dimensions Run Number 1	9
II.	Slug Calorimeter Locations and Dimensions Run Number 2	10
III.	Gardon Gage Locations and Dimensions Run Number 2	13
IV.	Test Conditions	27
V.	Estimated Data Precision	32

LIST OF FIGURES

FIGURE		PAGE
1.	AEDC-VKF Hypersonic Tunnel C	5
2.	Schematic of Model	7
3.	Slug Calorimeter Schematic	8
4.	Gardon Gage Schematic	12
5.	Cylindrical Coordinate System Applied to a Calorimeter Slug	15
6.	Temperature History of Slug Front and Rear Surfaces	18
7.	Schematic of Gardon Gage Sensing Disc Element	22
8.	Time Variation of Supramica Insulated Slug Calorimeter Indicated Heat Transfer	34
9.	Time Variation of Semicon Insulated Slug Calorimeter Indicated Heat Transfer	35
10.	Time Variation of Nylon Insulated Slug Calorimeter Indicated Heat Transfer	36
11.	Time Variation of Indicated Heat Transfer from Supramica Insulated Slug Calorimeter with Small Slug	39
12.	Comparison of Theoretical and Gardon Gage Experimental Stagnation Point Heat Transfer	41
13.	Effect of Sensing Disc Thickness on Gardon Gage Indicated Heat Transfer, D = 0.250 Inches	42

FIGURE PAGE

14. Effect of Sensing Disc Thickness on Gardon Gage Indicated Heat Transfer, D = 0.187 Inches 43

15. Effects of Sensing Disc Thickness on Gardon Gage Indicated Heat Transfer, D = 0.125 Inches 44

16. Summary Comparison of Gardon Gage Data with Theoretical and Experimental Heat Transfer Distributions 45

NOMENCLATURE

B	Thermocouple thermo-electric power, MV./°R
C_1	Slug calorimeter calibration factor, BTU/ft.^{2}-MV.
C_2	Gardon gage calibration factor, BTU/MV.
C_p	Specific heat, BTU/lb.-°R
d	Model diameter, in.
D	Slug or sensing disc diameter, in.
E	Thermocouple output, MV.
h	Heat transfer coefficient, BTU/ft.^{2}-sec.-°R
H	Total enthalpy, BTU/lb.
k	Thermal conductivity, BTU/ft.-sec.-°R
ℓ	Slug or sensing disc thickness, in.
L	Lewis number
M	Mach number
Nu	Nusselt number
p	Pressure, psia
Pr	Prandtl number
$\dot{q}$	Heat transfer rate, BTU/ft.^{2}-sec.
r	Radius, in.
R	Gardon gage sensing disc radius, in.
Re	Reynolds number
R_N	Model nose radius, in.
S	Surface distance in plane including model axis, in.
St	Stanton number

t	Time, sec.
T	Temperature, °R
T_c	Gardon gage sensing disc center temperature, °R
T_s	Steady state temperature, °R
u	Velocity, ft./sec.
x	Distance into calorimeter slug from back surface, in.
α	Thermal diffusivity, ft.^{2}/sec.
γ	Ratio of specific heats
θ	Angular location in the plane containing model axis, deg.
μ	Viscosity, lb.-sec./ft.^{2}
ρ	Density, lb./ft.^{3}
τ	Gardon gage time constant, sec.
ϕ	Angular location in the plane normal to the model axis, deg.
Ψ	Fourier modulus
ω	Viscosity parameter
$( )'$	Conditions behind a normal shock
$\dot{( )}$	First derivative with respect to time

Subscripts

FR	Fay and Riddell theoretical value
i	Initial conditions at $t = 0$
0	Stilling chamber conditions
w	Conditions at model surface
δ	Conditions at boundary layer edge
∞	Free-stream conditions

CHAPTER I

INTRODUCTION

Blunt nosed aerodynamic configurations have become commonplace among high speed vehicles which cannot withstand high surface heating. Of course, there is a drag penalty which must be dealt with, but the combination of low heating and high drag is particularly attractive to designers of reentry vehicles. Manned orbital vehicles such as Mercury, Gemini, Apollo and Vostok all utilize an extremely blunt heat shield section. Theoretical estimates of the heat transfer and pressure distributions over the blunt body and experimental wind tunnel data are used by the vehicle designers to establish structural requirements.

The most conventional type of model used to obtain heat transfer data in continuous flow wind tunnels are formed from sheet metal approximately 0.030 to 0.050 inches thick. The temperature of this thin shell is measured with thermocouples which are welded on the inner surface. A thin skin is required so that the thermocouples can respond quickly to the convective heat input before conduction along the skin introduces errors. The model designer must produce a model which will not distort or collapse under the external aerodynamic load and which does not have internal structure that acts as a heat sink. It is also significant that properly formed

model shells are expensive as well as fragile.

The model designers' problems would be greatly simplified if sturdy models with small calorimeters inserted in the thick walls could be used. Ledford (1)[1] described such an arrangement for obtaining data in short duration wind tunnels, but when similar insulated mass calorimeters or slug calorimeters were applied to obtain data in a continuous flow wind tunnel, the results were highly time dependent because of heat losses from the slug. The data were corrected for these losses, but it would be much more convenient if such corrections were not necessary. Experimental data presented in this study were obtained using a variety of slug calorimeters as well as asymptotic calorimeters.

Westkaemper (2) studied the possible sources of error caused by placing a calorimeter in a surface and divided the potential problem areas into two categories. The two categories could be termed geometric simulation and thermal simulation. The first category indicates that the body surface contour should not be changed by the installation of the calorimeter or the local heating rate will not be the same as it would be if the calorimeter were not present. If there is any curvature in the model surface this requirement cannot be rigidly adhered to and the most reasonable approach seems

[1]Numbers in parentheses refer to similarly numbered references in the bibliography.

to be to minimize the size of the calorimeter and exercise reasonable care while installing the calorimeter.

Thermal simulation dictates that the temperature across the face of the calorimeter should not represent a discontinuity in the body temperature distribution. Conti (3) and Rubesin (4) both showed that great errors in local heat transfer can be caused by a temperature mismatch between a calorimeter and the surrounding wall. The most practical approach to thermal simulation appears to be to limit the temperature rise of the calorimeter during a test run either by proper geometric design of the calorimeter or by reducing the test run time.

The objective of this study is to obtain heat transfer data on a blunt body with calorimeters and to determine if the data are precise enough to be useful.

CHAPTER II

APPARATUS

I. WIND TUNNEL

The experimental data reported in this thesis were obtained in the Gas Dynamic Wind Tunnel, Hypersonic (C), at the von Karman Facility of the Arnold Engineering Development Center. Tunnel C is a continuous, closed-circuit, variable density wind tunnel with an axisymmetric contoured nozzle and a 50-in.-diameter test section. This test was conducted at a nominal Mach number of 10 at stagnation conditions from 500 to 1800 psia. A stagnation temperature up to 1850 °R was utilized to prevent liquefaction of the air in the test section. The above operating conditions resulted in free-stream unit Reynolds numbers from 0.31×10^6 to 1.04×10^6 per foot. Tunnel C and its associated equipment are shown in Figure 1. The test section tank and safety doors allow the model to be injected into the test section for a test run and then retracted for model cooling or model changes without interrupting the tunnel flow.

A more complete description of Tunnel C can be found in References 5 and 6.

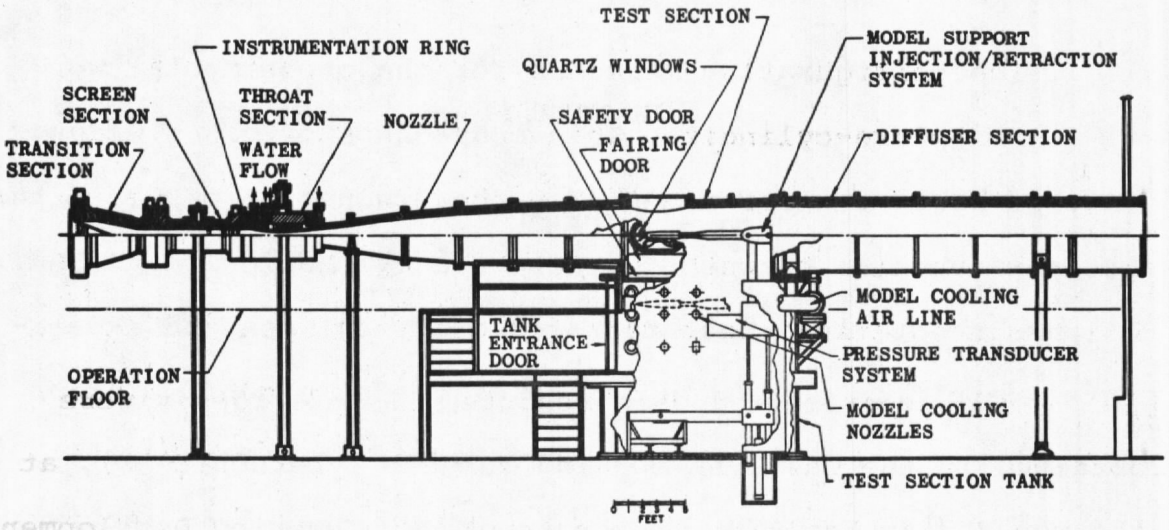

a. Tunnel Assembly

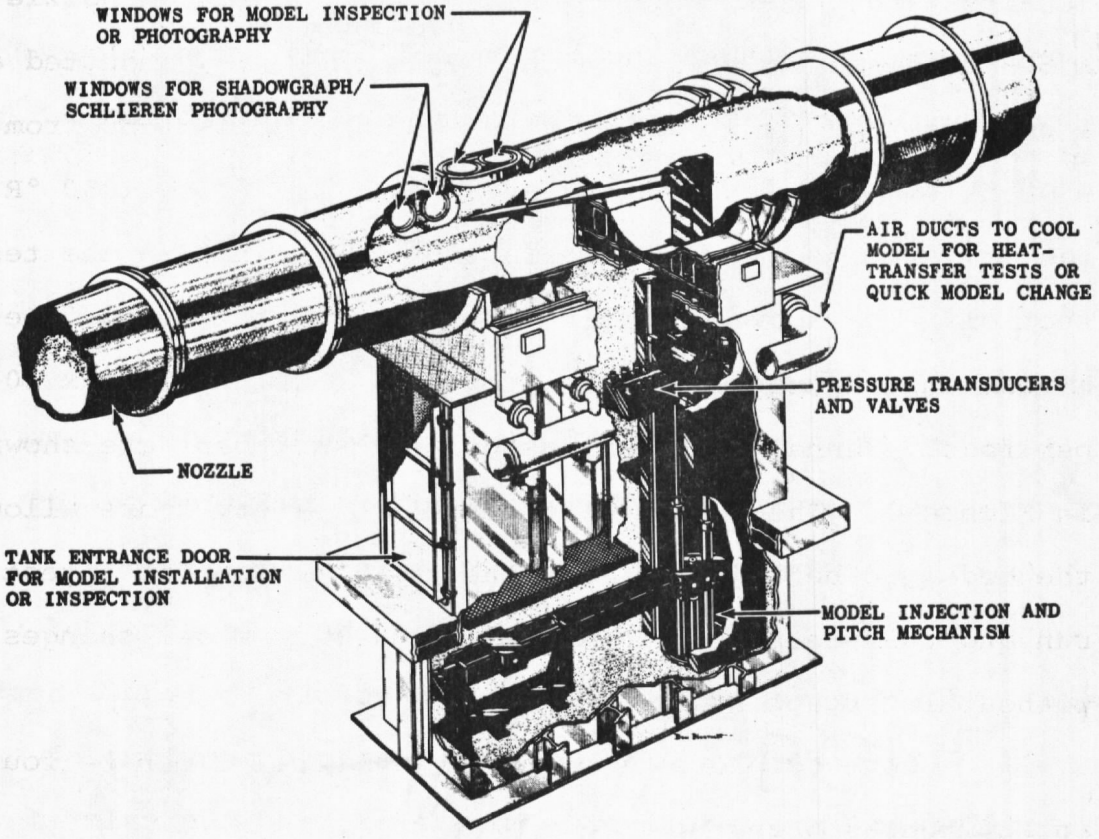

b. Tunnel Test Section

Figure 1. AEDC-VKF hypersonic tunnel C.

II. MODEL

The configuration selected for the experimental work was a hemisphere-cylinder. This body shape offers a wide range of heat transfer rates from the stagnation point to the shoulder junction between the nose and cylindrical afterbody. Reliable theoretical heat transfer distributions and experimental data from thin-skin models of the same configuration are both available with which to compare the present data.

The model, illustrated in Figure 2, was 5.80 inches in diameter and was constructed of Type 17-4 stainless steel. The model shell was machined from solid material; this a much simpler operation than forming a shell only a few thousandths of an inch thick. The calorimeters were lightly pressed into holes drilled in the shell.

III. CALORIMETERS

Slug Calorimeters

Several variations of an insulated mass calorimeter or slug calorimeter were investigated in two test periods. A typical slug calorimeter used in this study is shown in Figure 3. The insulator material and the dimensions of the slug and insulator were varied in an effort to reduce heat losses from the slug. The characteristic dimensions of the calorimeters, the calorimeter materials, and the calorimeter locations on the model from the first and second tests are shown in Table I and Table II, respectively.

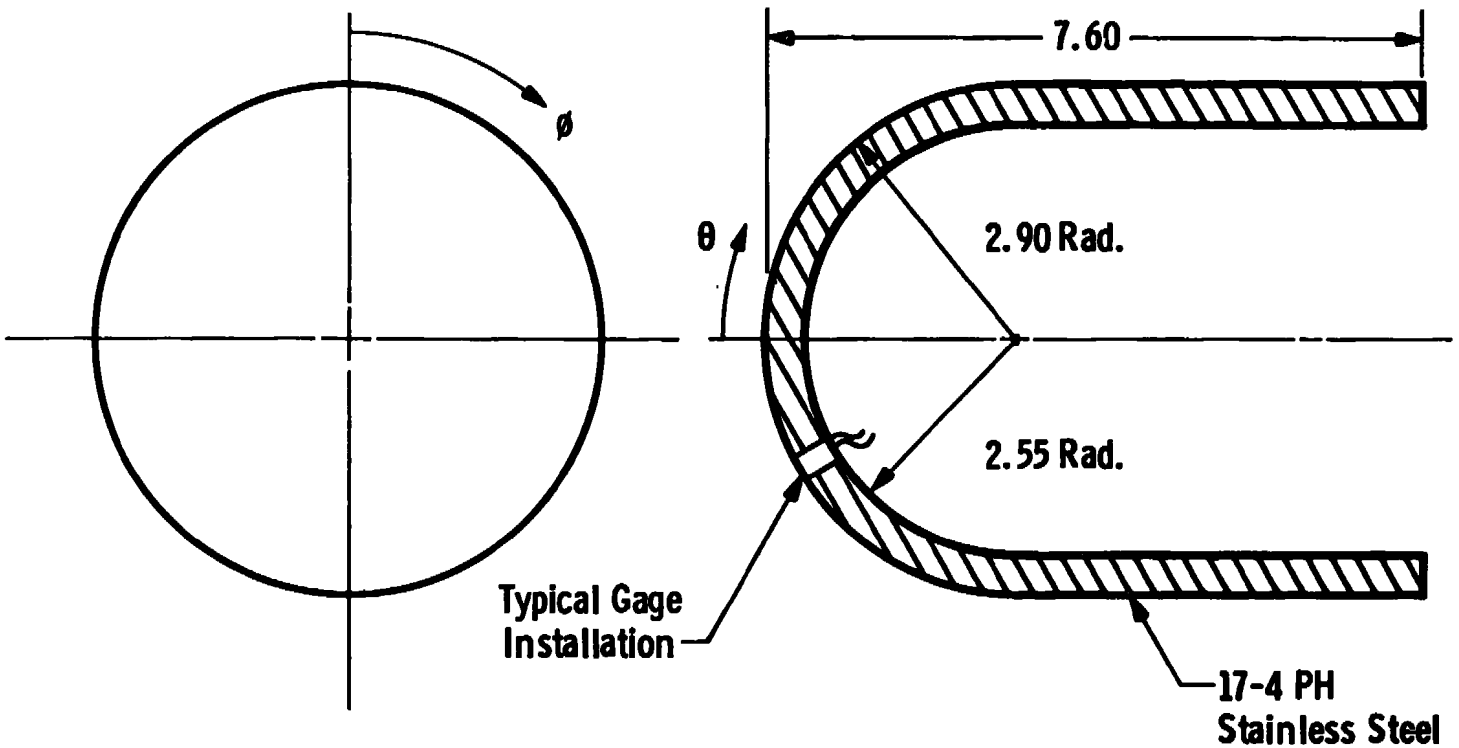

Figure 2. Schematic of model.

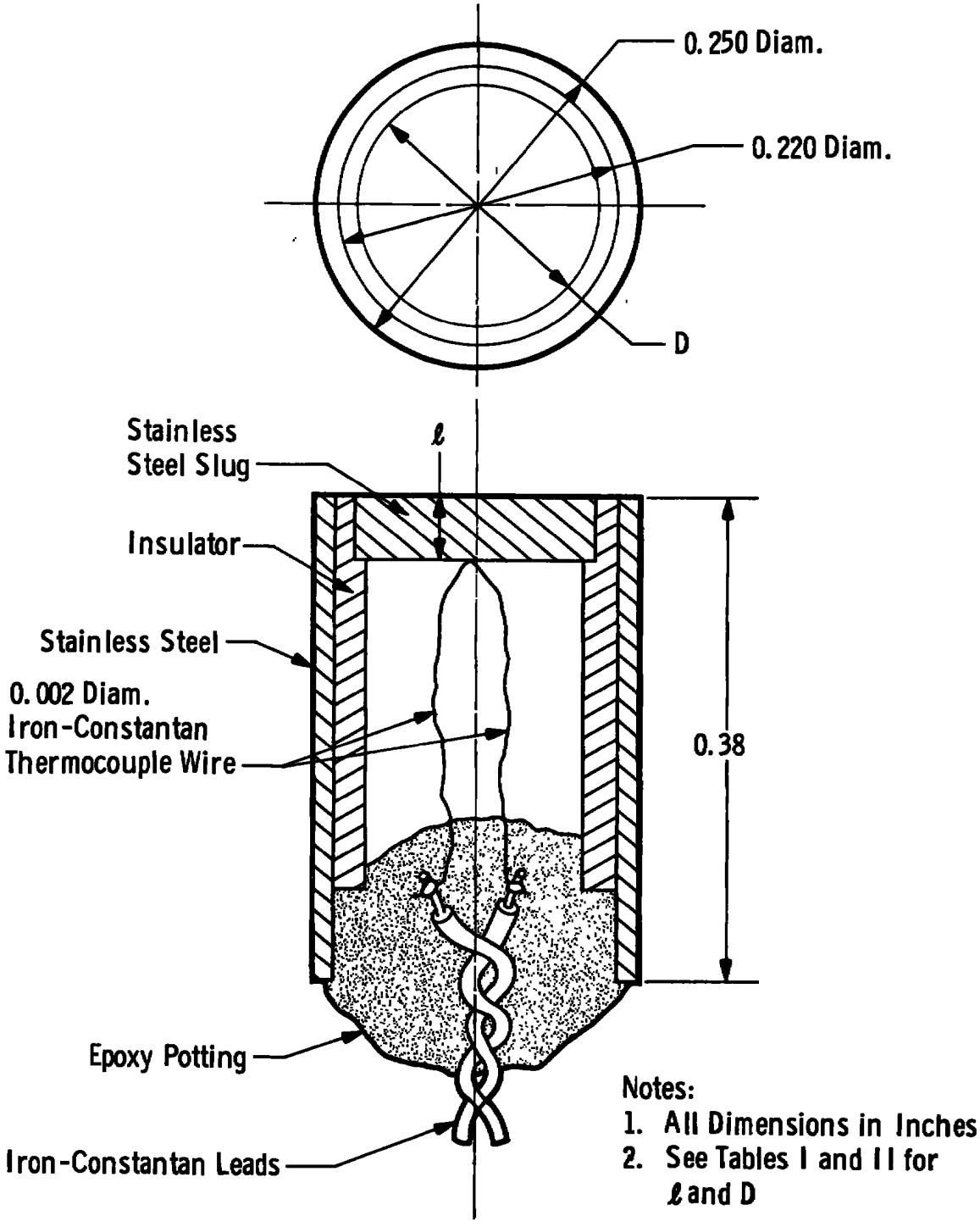

Figure 3. Slug calorimeter schematic.

TABLE I

SLUG CALORIMETER LOCATIONS AND DIMENSIONS
RUN NUMBER 1

ϕ, deg.	θ, deg.	S/R_N	D, in.	ℓ, in.	Insulator
0	60	1.048	0.125	0.050	Semicon
	75	1.310	0.187	0.050	Supramica
	90	1.572	0.187	0.050	Semicon
45	45	0.786	0.125	0.050	Semicon
90	30	0.524	0.187	0.050	Semicon
	45	0.786	0.187	0.050	Semicon
	60	1.048	0.187	0.050	Semicon
	75	1.310	0.125	0.050	Supramica
	90	1.572	0.187	0.050	Supramica
135	45	0.786	0.187	0.050	Supramica
180	30	0.524	0.125	0.050	Supramica
	45	0.786	0.125	0.050	Supramica
	60	1.048	0.187	0.050	Supramica
	75	1.310	0.125	0.050	Semicon
225	15	0.262	0.187	0.050	Semicon
	45	0.786	0.125	0.050	Supramica
270	45	0.786	0.125	0.050	Semicon
315	15	0.262	0.187	0.050	Supramica

TABLE II

SLUG CALORIMETER LOCATIONS AND DIMENSIONS
RUN NUMBER 2

ϕ, deg.	θ, deg.	S/R_N	D, in.	ℓ, in.	Insulator
180	15	0.262	0.187	0.100	Nylon
	30	0.524	0.187	0.100	Nylon
	45	0.786	0.187	0.100	Nylon
	60	1.048	0.187	0.100	Nylon
	75	1.310	0.187	0.100	Nylon
	90	1.572	0.187	0.100	Nylon

Gardon Gages

The type of asymptotic calorimeter used in this study was named after its originator who first described the device in Reference (7). Figure 4 shows the physical characteristics of this type of gage. The Gardon gage is a steady state instrument originally designed as a radiometer which could measure radiant heat flux input directly. Heat flows radially through the disc to the copper case which is the main gage structural member and a heat sink. A copper wire is attached to the center of the disc forming a thermocouple junction. A thermocouple system is then available, consisting of the copper wire, constantan disc, and copper case, which measures the temperature difference between the center and edge of the constantan disc. Therefore, the gage electrical output is proportional to the radial differential temperature which is a function of the heat input. Table III shows the characteristic dimensions of the Gardon gages used in this study and their respective positions on the test model.

IV. INSTRUMENTATION

A time history of the calorimeter electrical outputs was recorded on magnetic tape by a Beckman 210. The tape was then transferred to a CDC 1604 B computer which performed the data reduction using the equations in Chapter IV.

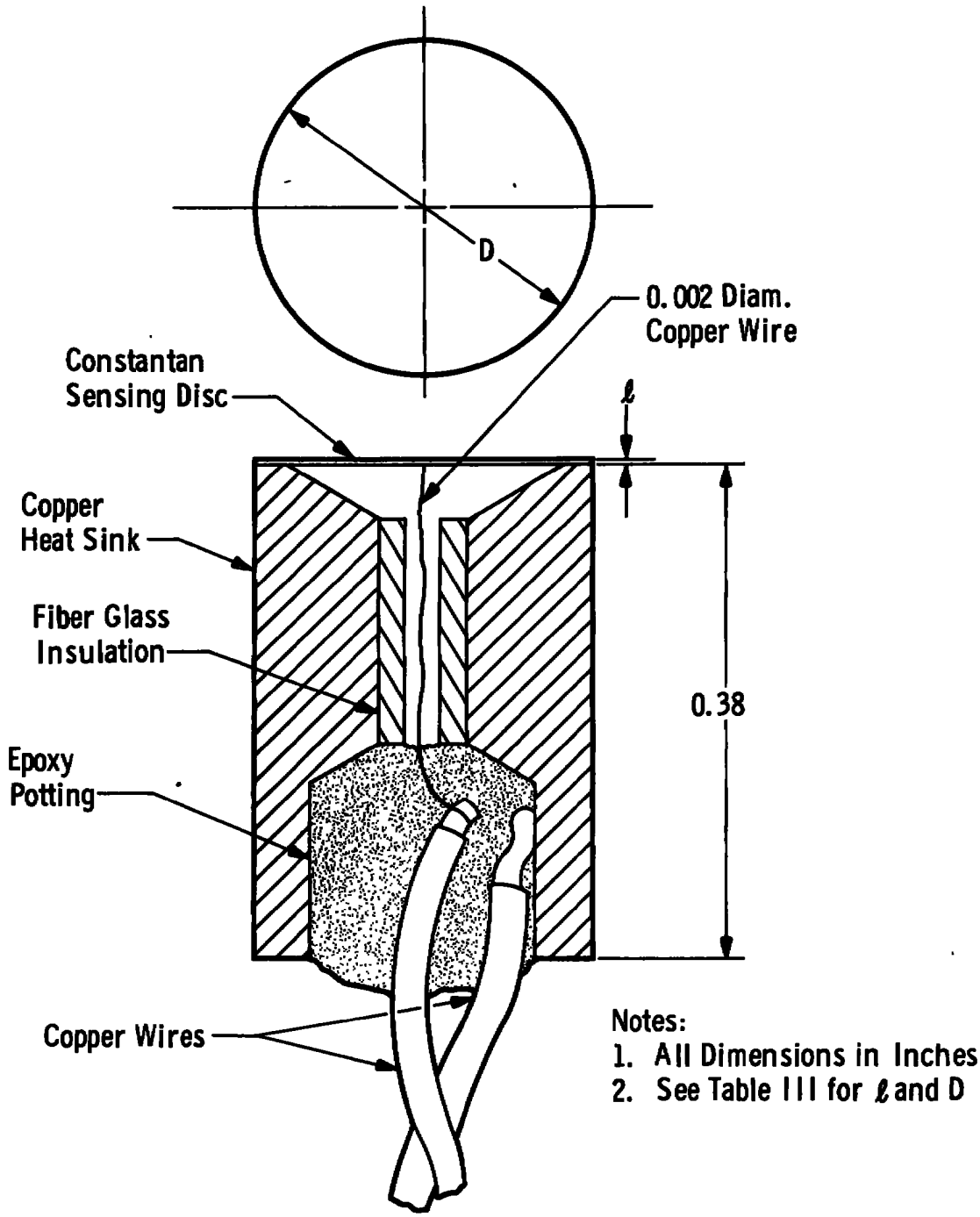

Figure 4. Gardon gage schematic.

TABLE III

GARDON GAGE LOCATIONS AND DIMENSIONS
RUN NUMBER 2

ϕ, deg.	θ, deg.	S/R_N	D, in.	ℓ, in.
0	0	0	0.250	0.020
	15	0.262	0.250	0.020
	30	0.524	0.250	0.020
	45	0.786	0.250	0.020
	60	1.048	0.250	0.020
	75	1.310	0.250	0.020
	90	1.572	0.250	0.010
45	15	0.262	0.125	0.005
	30	0.524	0.125	0.002
	60	1.048	0.125	0.002
	75	1.310	0.125	0.002
	90	1.572	0.125	0.002
90	15	0.262	0.250	0.020
	30	0.524	0.250	0.010
	45	0.786	0.250	0.010
	60	1.048	0.250	0.005
	75	1.310	0.250	0.005
	90	1.572	0.250	0.002
135	15	0.262	0.187	0.010
	30	0.524	0.187	0.005
	60	1.048	0.187	0.005
	75	1.310	0.187	0.002
	90	1.572	0.187	0.002
225	30	0.524	0.187	0.005
270	15	0.262	0.250	0.010
	30	0.524	0.250	0.020
	45	0.786	0.250	0.010
	60	1.048	0.250	0.010
	75	1.310	0.250	0.005
	90	1.572	0.250	0.002

CHAPTER III

CALORIMETER THEORY

I. SLUG CALORIMETER

The heat flow in a slug may be described by the following expression:

$$\nabla^2 T = \frac{\rho C_p}{k} \frac{\partial T}{\partial t} \tag{1}$$

Expanded in cylindrical coordinates, Equation 1 becomes

$$\frac{1}{r} \frac{\partial}{\partial r} \left(r \frac{\partial T}{\partial r} \right) + \frac{1}{r^2} \frac{\partial^2 T}{\partial \theta^2} + \frac{\partial^2 T}{\partial x^2} = \frac{\rho C_p}{k} \frac{\partial T}{\partial t} \tag{2}$$

where the coordinate system is defined in Figure 5. Assuming symmetrical heat flow, Equation 2 can be written as

$$\frac{1}{r} \frac{\partial}{\partial r} \left(r \frac{\partial T}{\partial r} \right) + \frac{\partial^2 T}{\partial x^2} = \frac{\rho C_p}{k} \frac{\partial T}{\partial t} \tag{3}$$

If the slug thickness, ℓ, is considered small it seems reasonable to assume that the derivatives of the temperature with respect to the radius or time are independent of x. Hence, Equation 3 can then be integrated with respect to x and solved for $\partial T/\partial x)_{\ell}$.

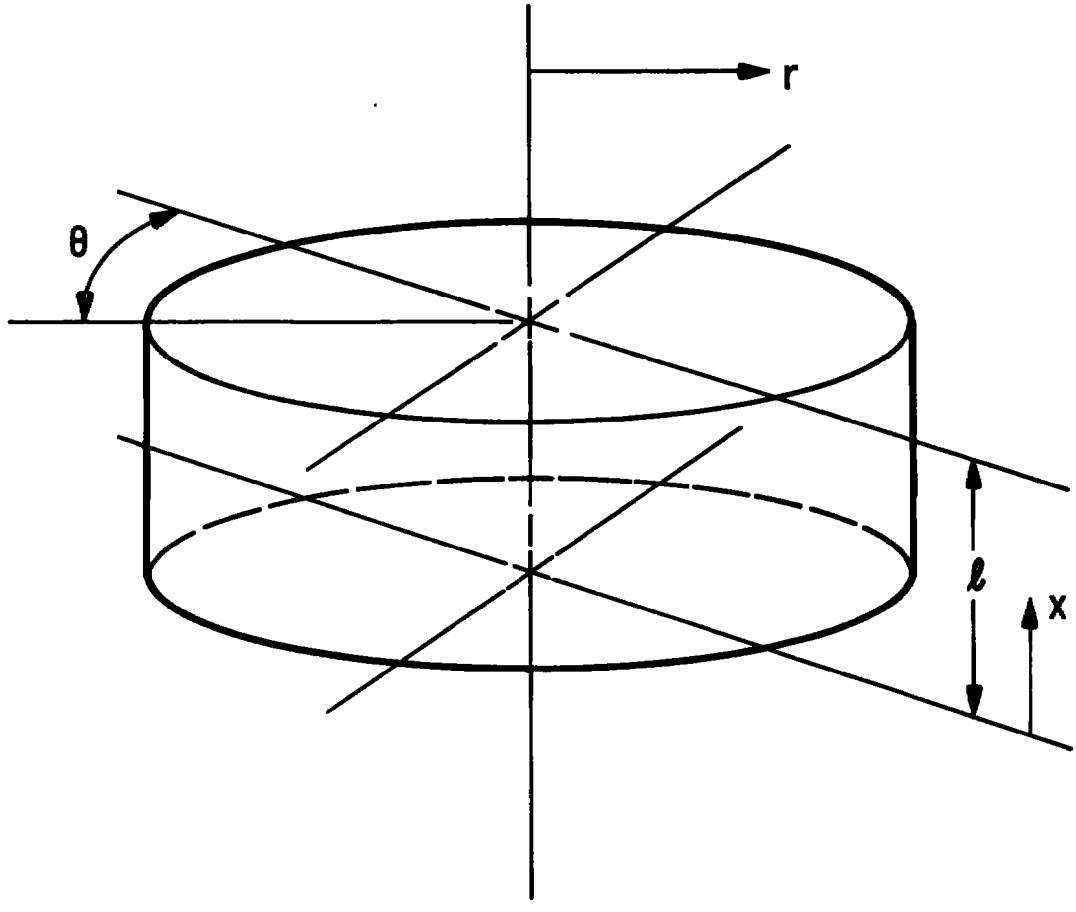

Figure 5. Cylindrical coordinate system applied to a calorimeter slug.

The result is

$$\left(\frac{\partial T}{\partial x}\right)_{\ell} = \frac{\rho C_p \ell}{k} \frac{\partial T}{\partial t} - \frac{\ell}{r} \frac{\partial}{\partial r}\left(r \frac{\partial T}{\partial r}\right) \tag{4}$$

where the boundary condition $\partial T/\partial x = 0$ at $x = 0$ has been applied. At the outer surface of the slug, $x = \ell$, the heat transfer to the slug is described by

$$\dot{q} = k\left(\frac{\partial T}{\partial x}\right)_{\ell} \tag{5}$$

Substituting Equation 4 into Equation 5, a final expression for the surface heat transfer may be written as

$$\dot{q} = \rho C_p \ell \frac{\partial T}{\partial t} - \frac{k\ell}{r} \frac{\partial}{\partial r}\left(r \frac{\partial T}{\partial r}\right) \tag{6}$$

The first term on the right side of Equation 6 represents the net local heat storage if no conduction was present. The second term represents the radial conduction away from the center of the slug. If the temperature difference between the slug and the insulation remains small, the conduction term can be considered very small compared to the storage term. Therefore, Equation 6 can be further simplified to the following

$$\dot{q} = \rho \ell C_p \frac{dT}{dt} \tag{7}$$

Additional assumptions employed in the derivation of Equation 7 are:

1. Radiation losses from the slug to the cold tunnel walls are negligible.
2. Conduction losses down the thermocouple wire are negligible.
3. The temperature gradient through the slug is small.

A liberal estimate revealed that less than 0.20 per cent of the heat input to the slug was lost through radiation. Similarly generous estimates yielded an extremely small conduction loss down the thermocouple wires. Consequently, radiation and wire conduction losses do appear negligible.

Kurzrock (8) considered the validity of assuming no temperature gradient through the slug by approximating the slug with a semi-infinite slab. The temperature distribution through the slug resulting from a suddenly applied heat input is

$$T = 2\dot{q}\sqrt{\frac{t}{k\rho C_p}} \sum_{n=0}^{\infty} \left[i\,\mathrm{erfc}\left(\frac{(2n+1) + x/\ell}{2\sqrt{\Psi}} \right) + i\,\mathrm{erfc}\left(\frac{(2n+1) - x/\ell}{2\sqrt{\Psi}} \right) \right] \tag{8}$$

A comparison of the temperature history of the front and back surfaces of the slug is shown in Figure 6. Not only is there a temperature difference between the slug surfaces, but the

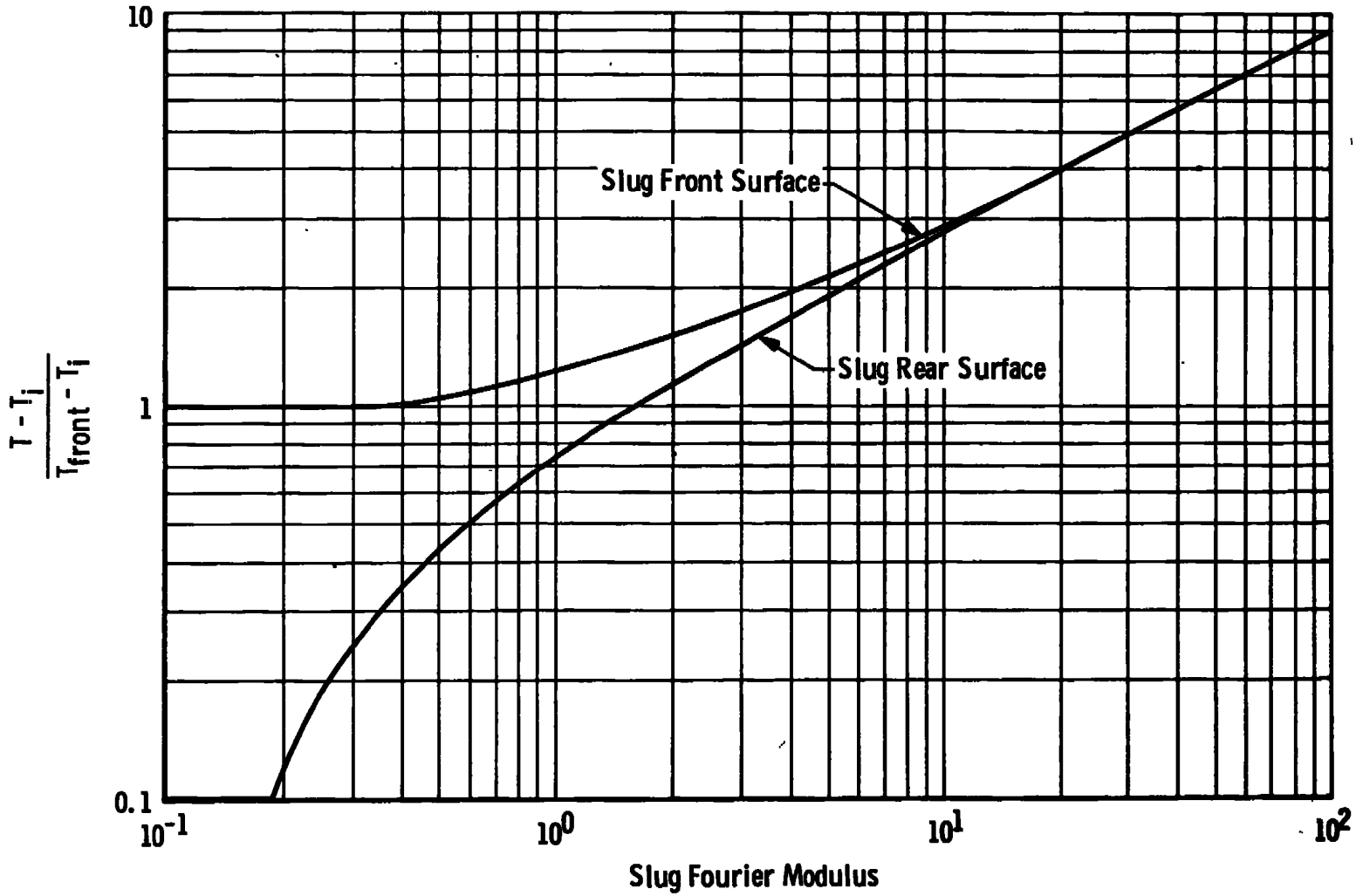

Figure 6. Temperature history of slug front and rear surfaces.

rate of temperature increase at the two surfaces is different. Since the calorimeter thermocouple indicates the rear face temperature, it is possible to choose an incorrect slope if the data are reduced too early in the test run. An additional error can be introduced when a wall temperature is selected to evaluate the heat transfer coefficient if the front and rear surface temperatures do not agree.

The Fourier modulus, Ψ, is a convenient parameter to use as a guide to choosing a proper data reduction time because it is a function of the thermal properties and dimensions of the slug and time. It is defined as

$$\Psi = \frac{\alpha t}{\ell^2} \tag{9}$$

where α is the thermal diffusivity. As Figure 6 shows, there is reasonably good agreement between the front and back surface temperatures and temperature history slopes for values of above approximately 10. After selecting a slug material, a value of Ψ can be chosen and a response time calculated in order to specify a data reduction time.

Caution should be exercised when applying Equation 8 because it was formulated assuming a suddenly applied step heat input. This condition is closely approximated in a short run blow down wind tunnel; however, injecting a model into the free-stream of a continuous flow wind tunnel subjects the model to unsteady initial heating as the model

passes through the tunnel boundary layer. Therefore, there is no clear approach to calculating a time for correct data reduction under the test conditions encountered in the present experimental work. Reference (9) offers a short approximation to Equation 8 which is convenient for quick estimates of slug calorimeter response times:

$$t \simeq -\frac{\ell^2}{\alpha\pi^2} \ln \left(\frac{1 - \frac{\dot{q}_{\text{indicated}}}{\dot{q}_{\text{input}}}}{2} \right) \tag{10}$$

The sensitivity of the calorimeter is a function of both the slug characteristics and the sensitivity of the rear face thermocouple. The thermo-electric output of the thermocouple may simply be described as

$$dE = B\, dT \tag{11}$$

Applying this expression to Equation 7 yields the calorimeter sensitivity

$$\frac{dE/dt}{\dot{q}} = \frac{B}{\rho \ell C_p} \tag{12}$$

As Equation 12 shows, the calorimeter sensitivity can be easily adjusted by varying the slug properties and thickness.

II. GARDON GAGE

A mathematical expression of the temperature in the sensing disc of a Gardon gage may be obtained by performing a heat balance on a differential element shown in Figure 7. The temperature of this element is described by the following:

$$\frac{\rho C_p}{k}\frac{\partial T}{\partial t} = \frac{\dot{q}}{\ell k} + \frac{1}{r}\frac{\partial T}{\partial r} + \frac{\partial^2 T}{\partial r^2} \tag{13}$$

Boundary conditions which apply to Equation 13 are:

1. $T = T_i$ at $t = 0$ and $0 < r < R$ and
2. $T = T_i$ at $0 < t < \infty$ and $r = R$

Equation 13 was derived under the following assumptions:

1. Radiation heat losses from both sides of the sensing disc are negligible.
2. Conduction heat loss down the center copper wire is negligible.
3. Sensing disc rear face convection heat losses are negligible.

The total radiation heat loss from both sides of the sensing disc is estimated to be less than 0.40 per cent of the total heat input to the disc. Estimates of the conduction heat loss down the center copper wire showed that this error was insignificant. The assumption of zero temperature gradient through the sensing disc also appears reasonable.

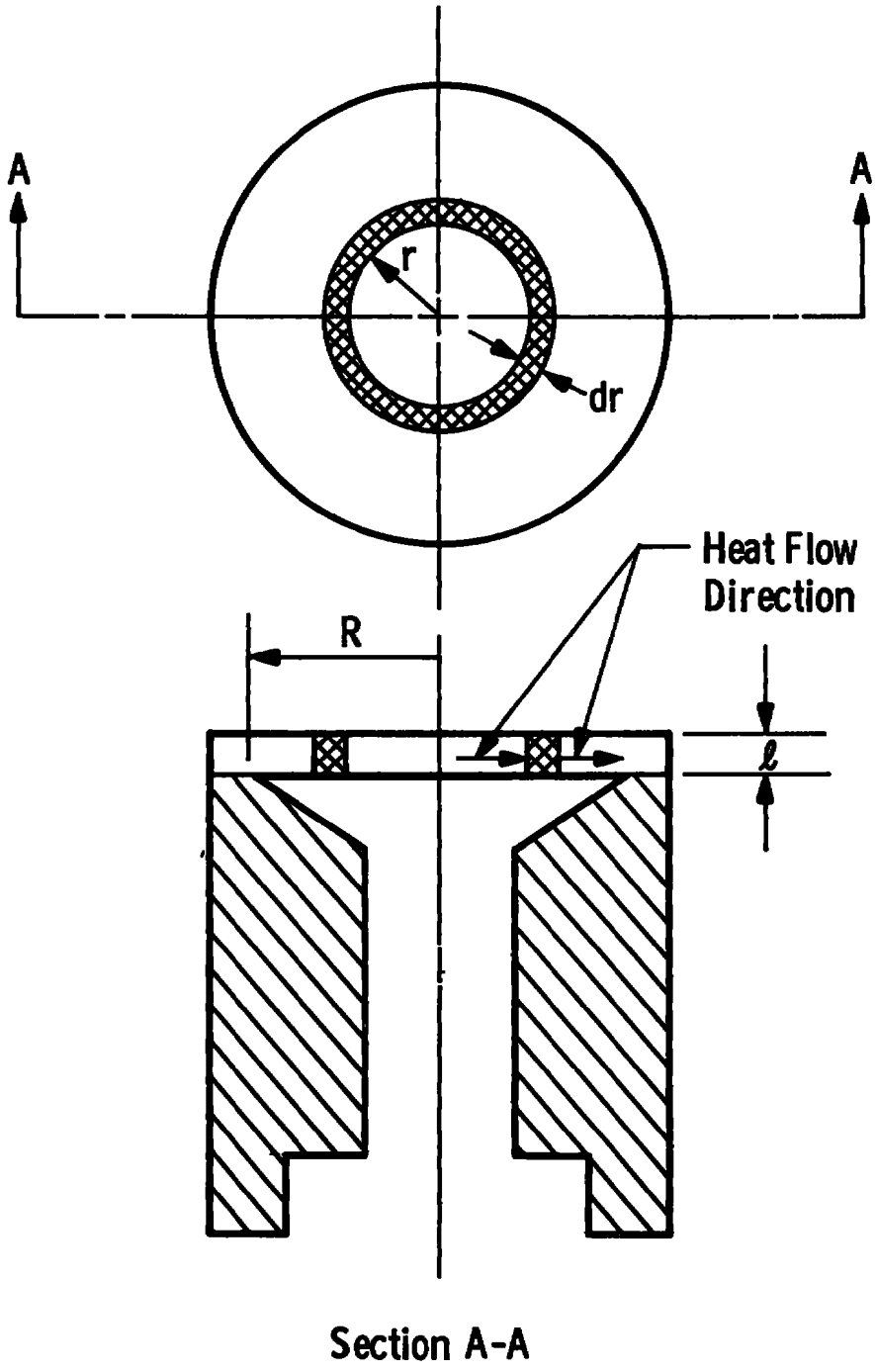

Figure 7. Schematic of Gardon gage sensing disc element.

Indeed, one second after an instantaneous heat flux is applied to the surface of an 0.020 inch thick constantan disc, the Fourier modulus is approximately 21. Figure 6, page 18, shows that there is virtually no temperature difference between the two surfaces of the sensing disc at the Fourier modulus of 21. Since 0.020 inch thick sensing discs were the thickest used in these experiments, this example should be the most severe test of the zero temperature gradient assumption.

The second boundary condition which specifies that the disc edge temperature at r = R remains constant is also an assumption. This assumption seems reasonable so long as the volume of the copper heat sink is much greater than the volume of the sensing disc.

An expression for the sensitivity of a Gardon gage may be obtained by determining the differential temperature which results from the application of a given heat flux input. The steady state temperature distribution in the sensing disc is

$$\frac{d^2T_s}{dr^2} + \frac{1}{r}\frac{dT_s}{dr} + \frac{\dot{q}}{k\ell} = 0 \qquad (14)$$

where T_s is the steady state temperature at radius r. The boundary conditions associated with Equation 14 are:

1. $T = T_i$ at $r = R$ and
2. $T = T_c$ at $r = 0$.

Applying these boundary conditions to the general solution, the sensitivity equation is

$$\Delta T = T_c - T_i = \frac{\dot{q}}{4k\ell} R^2 \tag{15}$$

The conductivity, k, was considered constant within the limited temperature range anticipated for ΔT. Introducing the thermo-electric power of a copper-constantan thermocouple into Equation 15, the final expression for sensitivity is

$$\frac{E}{\dot{q}} = \frac{BR^2}{4k\ell} \tag{16}$$

Gardon (7) approximated the rate of temperature rise of a Gardon gage sensing disc in the presence of a suddenly applied heat input as

$$T = T_c(1 - e^{-t/\tau}) \tag{17}$$

Equation 17 is actually an application of the concept of Newtonian heating. Schneider (10) defines the exponent, t/τ, as

$$\frac{t}{\tau} = \left(\frac{R}{\ell}\right)_{Nu} \Psi$$

where

$$Nu = \frac{hR}{k}$$

$$\Psi = \frac{kt}{C_p \rho R^2}$$

The instrument time constant, τ, becomes

$$\tau = \frac{C_p \rho}{4k} R^2 \qquad (18)$$

Combining Equations 17 and 18 reveals that less than 1.5 seconds are required for the largest diameter gage used in these experiments, D = 0.25 inches, to reach approximately 95 per cent of the steady state temperature.

It is evident that both the sensitivity and speed of response of a Gardon gage are strongly dependent on the sensing disc radius, R. Consequently, both of these characteristics can be controlled by adjusting the size of the gage. It is likewise beneficial that a smaller diameter gage more nearly satisfies the requirement for geometric simulation.

CHAPTER IV

PROCEDURE

I. TEST PROCEDURES

Test conditions for the present data are summarized in Table IV. At each listed test condition, the model was injected into the free-stream tunnel flow at a tunnel axial station which had a reasonably uniform pitot pressure distribution. Data were recorded for approximately five seconds before the model was retracted into the chamber beneath the tunnel test section. The model was then cooled to an isothermal condition before the next data run was started.

II. DATA REDUCTION

All data presented herein were reduced to a non-dimensionalized heat transfer coefficient, Stanton number, from the following expression:

$$St = \frac{\dot{q}}{\rho_\infty u_\infty (H_0 - H_w)} \tag{19}$$

The heat transfer rate, $\dot{q}$, for the slug calorimeters was computed as

$$\dot{q} = C_1 \, dE/dt \tag{20}$$

TABLE IV

TEST CONDITIONS

M_∞	p_0, psia	T_0, °R	p_∞, psia	$Re_{\infty_d} \times 10^{-6}$	Run
10.08	500	1850	0.0107	0.31	2
10.16	1000	1850	0.0203	0.60	1, 2
10.17	1200	1850	0.0246	0.73	1, 2
10.20	1800	1850	0.0365	1.04	1

where C_1 is the calorimeter calibration factor. Gardon gage heating rates were computed from the following expression:

$$\dot{q} = C_2 E \tag{21}$$

where C_2 is the gage calibration factor and E is the gage electrical output.

Data were recorded on magnetic tape at the rate of 20 times per second. A digital computer was used to fit a parabola through 21 consecutive voltage values centered about the specific point of interest. The voltage-time derivative, dE/dt, was obtained from the parabola to evaluate Equation 20. Data were reduced for the present study 0, 0.25, 0.50, 1.00, and 2.00 seconds measured from the time the model reached the centerline of the tunnel.

Total enthalpies, H_0 and H_w, were calculated using measured values of T_0 and T_w and the relationship

$$H = C_p T$$

where the specific heat, C_p, was assumed constant. The free-stream properties were corrected for real gas effects by using the Beattie-Bridgeman equation of state and the procedures specified in Reference 11. Slug calorimeter data were reduced using the indicated wall temperature to evaluate the total enthalpy, H_w. Gardon gage heat transfer

coefficients were reduced with the sensing disc center temperature:

$$T_c = T_{edge} + \Delta T \tag{22}$$

where T_{edge} was assumed constant at the initial temperature.

III. SLUG CALORIMETER AND GARDON GAGE CALIBRATION

Slug Calorimeters

All the slug calorimeters used in these experiments were calibrated with a known convective heat flux input from an oxy-acetylene torch as described in Reference 12. A reference calorimeter was also exposed to the same heat source and the combination of the reference calorimeter indicated heating rate and the test calorimeter electrical output yielded the calibration factor, C_1. The experimental value of C_1 agreed with the theoretical value, $\rho\ell C_p$, within approximately ± 5 per cent. Other information gained from the calibration procedure showed that the experimental response times were within ± 10 per cent of the theoretical predictions. Similarly, calorimeter sensitivity values computed from Equation 12 and experimental sensitivity values agreed with ± 5 per cent.

Gardon Gages

A radiant heat source consisting of six quartz-iodine

lamps was used to calibrate the Gardon gages. Low heat inputs were required to limit the temperature rise in the thin sensing discs. The lamp bank proved more controllable than a torch at low heating rates; consequently, it was selected as the heat source for the Gardon gage calibration procedure.

The lamps were mounted in a plane parallel to the gage sensing discs. A flat black Krylon^R coating was applied to the sensing discs which gave the surfaces a known absorptivity. The absorptivity of flat black Krylon^R is approximately constant near unity over the wave length range of the quartz-iodine lamps' emitted energy . A reference slug calorimeter and a Gardon gage were irradiated simultaneously; the resulting outputs were used to compute the Gardon gage calibration factor, C_2.

The experimental values of C_2 deviated from the theoretical value, $4k\ell/BR^2$, by approximately ± 5 per cent for the largest gages (D = 0.25 inches) to ± 20 per cent for the smallest gages (D = 0.125 inches). The inability to locate the center wire accurately probably produces enough uncertainty in the value of R to heavily influence the theoretical value of C_2. Experimental response times generally agreed with theoretical times within ± 10 per cent. Gage experimental sensitivities were within ± 10 per cent of the values computed from Equation 16.

IV. DATA PRECISION

Estimated precisions for the individual quantities required for complete data reduction are listed in Table V. An approximation of an overall data precision was made by computing a root-sum-squared error from the individual precision estimates. The results showed that both the slug calorimeter and Gardon gage data could be expected to have an approximate precision of ± 6 per cent so long as E and dE/dt remain above the minimum limits shown in Table V.

TABLE V

ESTIMATED DATA PRECISION

QUANTITY	ESTIMATED PRECISION
C_1	± 5%
C_2	± 5%
E	± 10 microvolts or ± 1%, whichever is greater
T_0	± 1%
T_w	± 1%
T_{edge}	± 1%
dE/dt	± 3% or ± 0.01 $\frac{MV}{sec}$, whichever is greater
p_∞	± 1%
u_∞	± 1%
C_p	± 1%

CHAPTER V

RESULTS AND DISCUSSION

All the data presented herein are non-dimensionalized with a theoretical stagnation point heat transfer coefficient formulated by Fay and Riddell (13) and compared with Lees' (14) heat transfer distribution. A brief description of these two theories and the numerical evaluation procedure is given in the Appendix.

I. SLUG CALORIMETER RESULTS

Typical slug calorimeter data are compared with Lees' predicted values in Figures 8 through 10. Data from calorimeters located at several different positions on the model are presented to illustrate the calorimeters' performance in the presence of various heat inputs. Regardless of the insulator material, all the data illustrated show a large variation with time, probably due to conduction losses from the slug. In addition, the initial point was considerably higher than Lees' value in all cases. Equation 10 indicates that all of the calorimeters had more than sufficient response time compared to the length of time required to inject the model into the free-stream flow; hence, the high initial point must have originated for some other reason.

Stagnation point data were obtained during

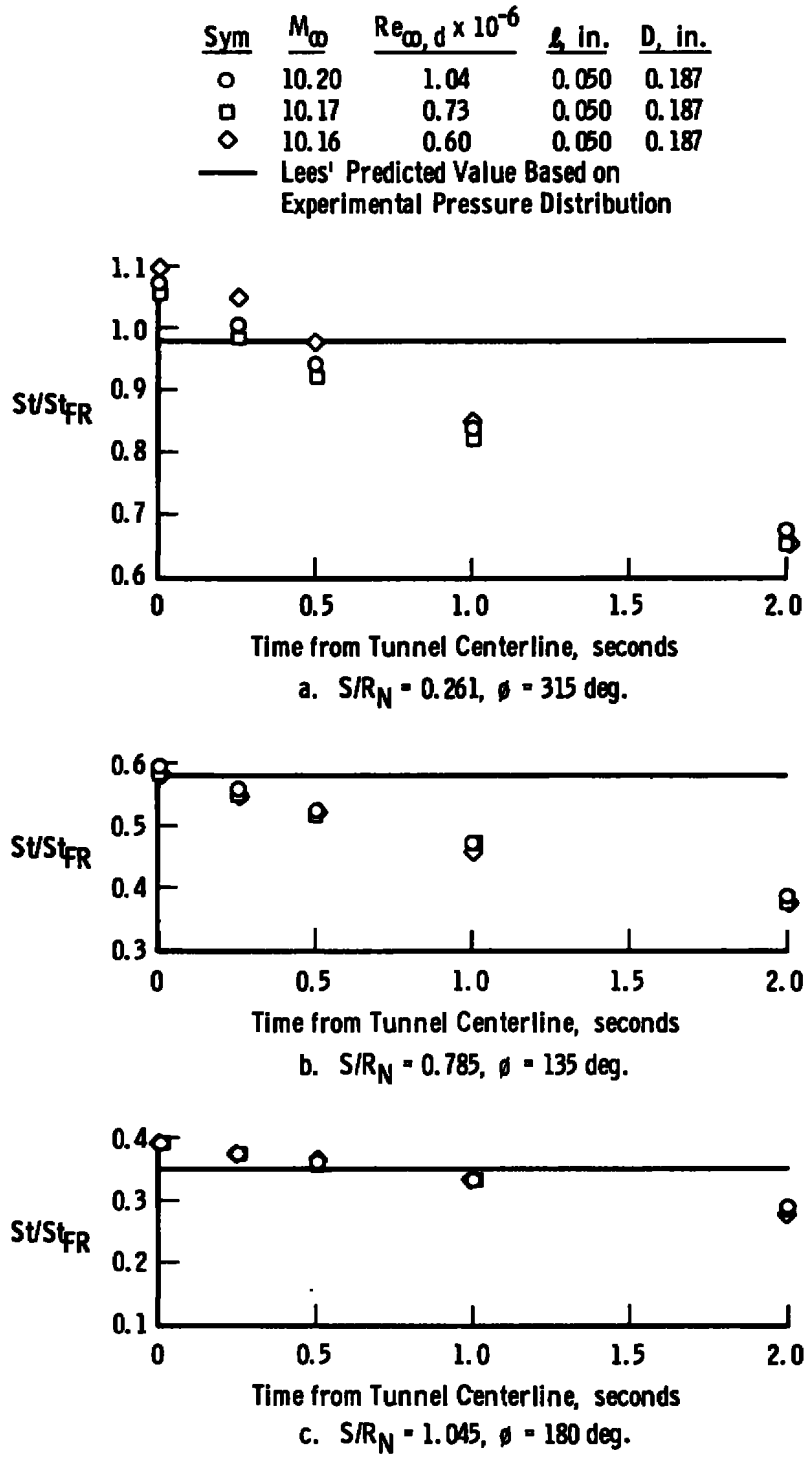

Figure 8. Time variation of Supramica insulated slug calorimeter indicated heat transfer.

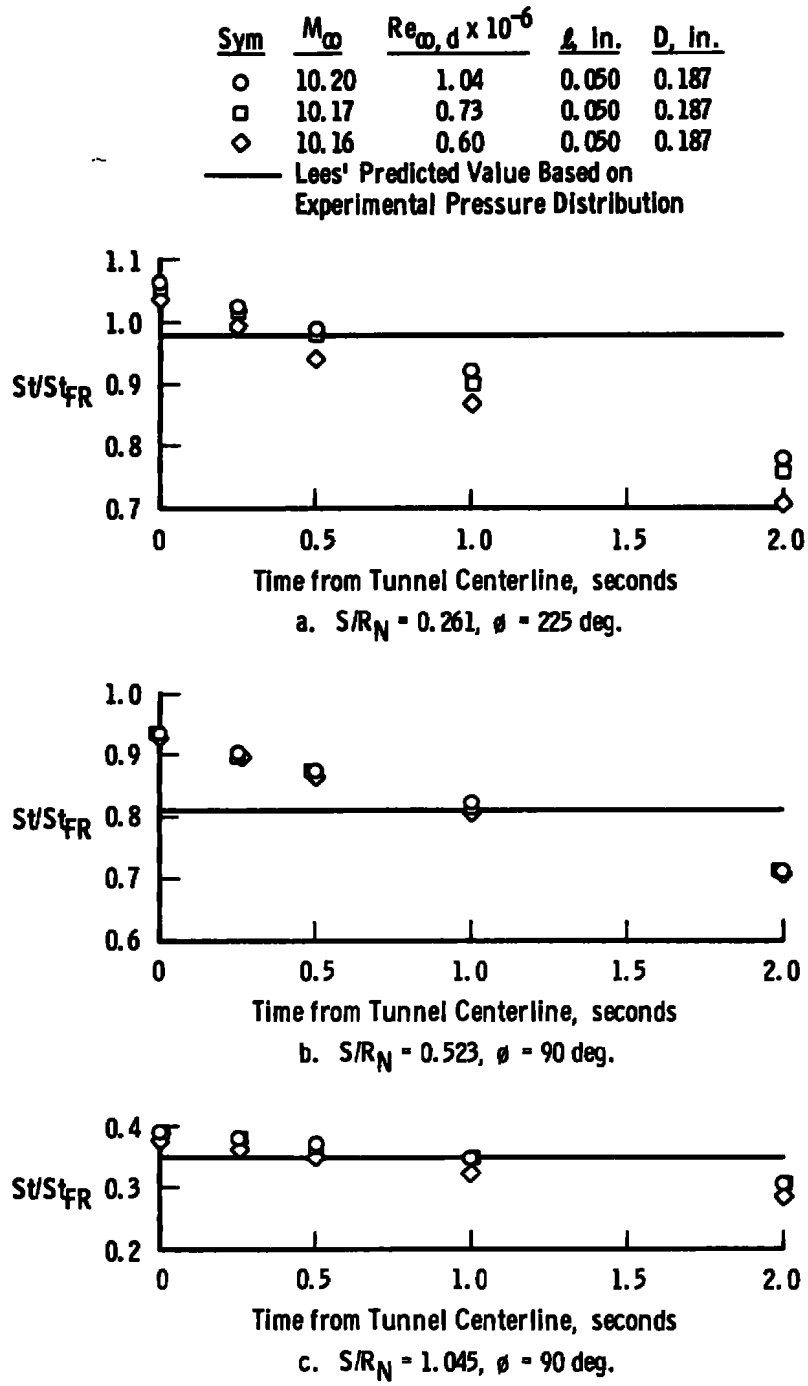

Figure 9. Time variation of Semicon insulated slug calorimeter indicated heat transfer.

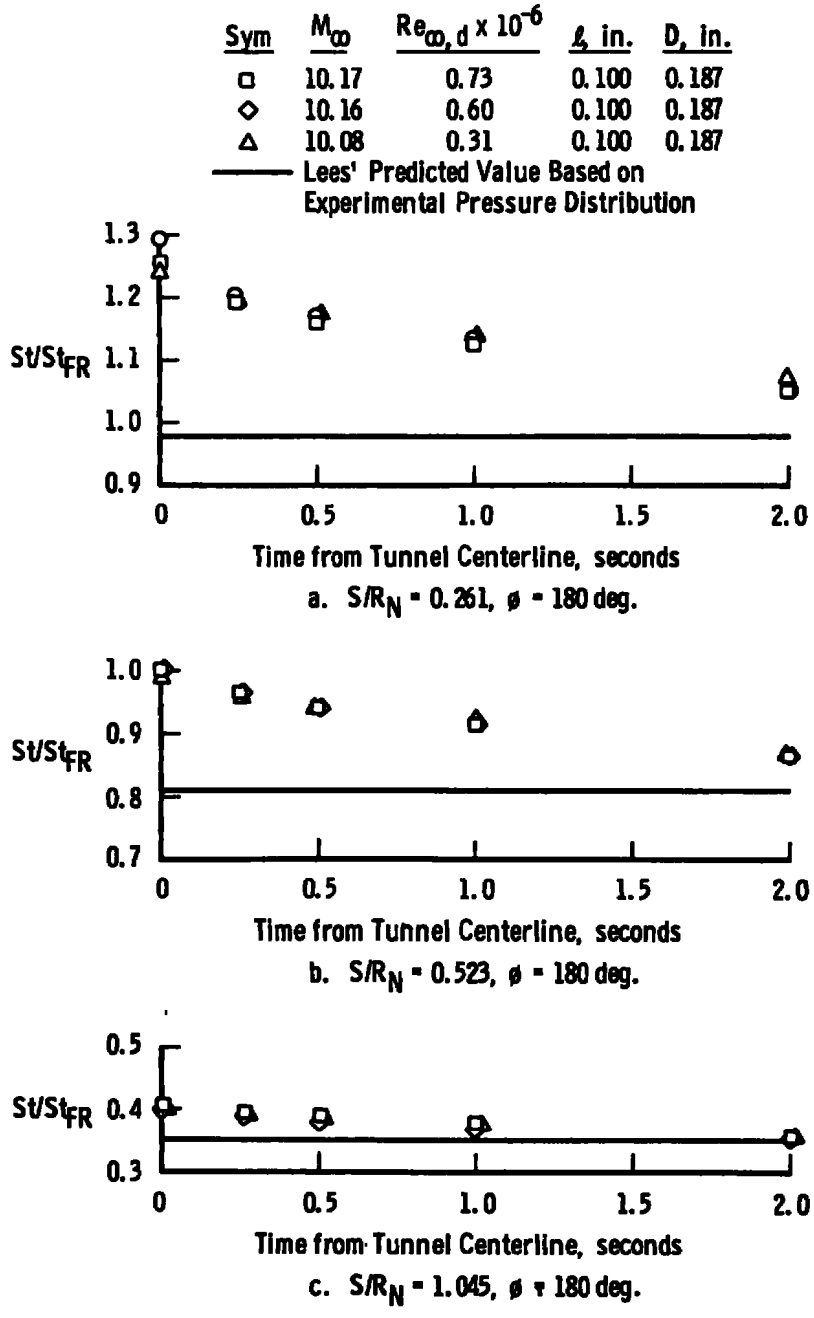

Figure 10. Time variation of nylon insulated slug calorimeter indicated heat transfer.

the injection motion using a 5.8 inch diameter hemisphere-cylinder model with a 0.040 inch thick skin. The indicated heat transfer rate rose to more than 50 per cent above Fay and Riddell's predicted value before dropping to near the correct value when the model reached the tunnel centerline. This peak heating characteristic was attributed to the interaction between the model bow shock and the wind tunnel boundary layer as the model traversed the tunnel boundary layer. This same phenomena may have been responsible for the excessively high indicated heat transfer rates at t = 0. The heat pulse had the additional detrimental contribution of causing the differential temperature between the slug and the surrounding insulator to increase rapidly before the model reached the tunnel centerline, thereby allowing an early onset of radial conduction losses. Conduction losses apparently caused the downward trend in the indicated heat transfer coefficients.

Westkaemper (2) performed a numerical analysis of the temperature distribution in the insulator and a slug of a slug calorimeter subjected to a suddenly applied heat input. His results showed that the surface temperature of the insulator may exceed the surface temperature of the slug for a short time after the heat is applied if the insulator thermal diffusivity is much less than the slug thermal diffusivity. Consequently, heat conduction into the slug can occur which may also contribute to the high early

indicated heat transfer rates. This is particularly true for the nylon insulated calorimeters, since the thermal diffusivity of nylon is lower than either Semicon^{R} or Supramica^{R}.

An effort was made to reduce the radial conduction losses by increasing the radial thickness of the insulation. The 0.25 inch outside diameter was maintained and the slug diameter was reduced from 0.187 inches to 0.125 inches. The resulting data, presented in Figure 11, show that conduction losses increased rather than decreased. The initial point (t = 0) was very high and the rate of decrease in the indicated heat transfer coefficient was slightly greater than the results from calorimeters with large slugs. Increasing the surface area of the insulator may have allowed heat to flow into the slug and caused the initial data point to be high. Reduction of the slug volume allowed the slug temperature to rise more rapidly than a large slug and promoted the onset of radial conduction losses.

Perhaps the greatest obstacle to success in these slug calorimeter experiments was the requirement for injecting the model into the wind tunnel free-stream through the tunnel boundary layer. If the test model could be equipped with a disposable insulating shield which could be jettisoned after the model passed through the tunnel boundary layer, it seems reasonable to speculate that usable data could be obtained. Otherwise, conduction heat losses must be accounted

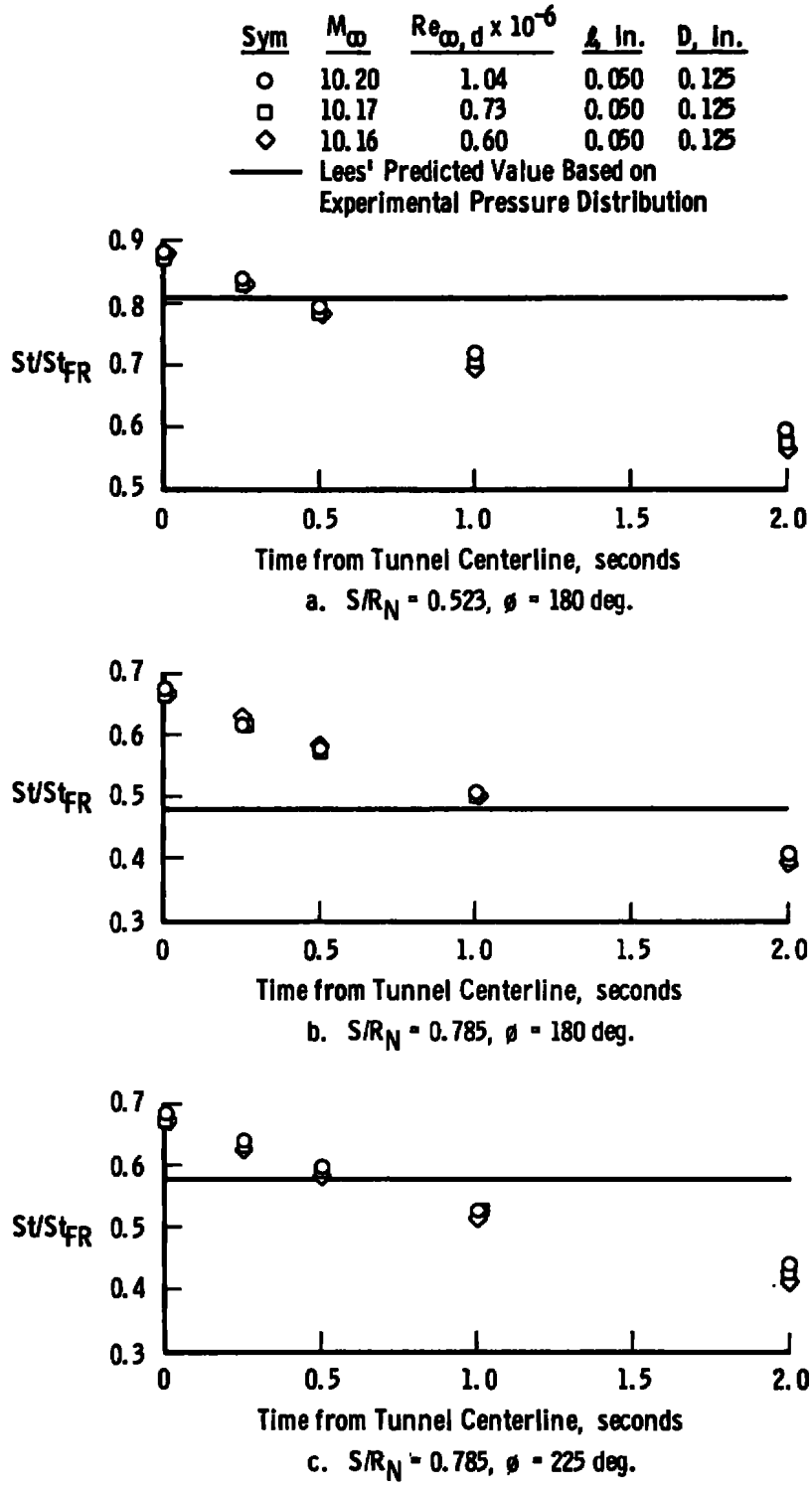

Figure 11. Time variation of indicated heat transfer from Supramica insulated slug calorimeter with small slug.

for.

II. GARDON GAGE RESULTS

Experimental Gardon gage heat transfer data are compared with theoretical heat transfer distributions and with previous thin-skin data in Figures 12 through 16. There was no data deviation which appeared to be a function of either model or flow malalignment; therefore, all the data are plotted without regard for the circumferential location of the gages. Gage response estimates indicated that the gages probably would not reach steady state operation until the model had been on the tunnel centerline for 0.50 to 0.75 seconds. However, an oscillograph trace of several gage outputs during the injection motion showed that the gages actually reached steady state operation before the model arrived on the tunnel centerline. The model bow shock-tunnel boundary layer interaction probably caused the gage sensing disc temperature to rise more rapidly than estimates indicated. Consequently, all the Gardon gage data presented were recorded when the model reached the wind tunnel centerline.

A comparison among the present Gardon gage experimental stagnation point heat transfer, Fay and Riddell's (13) predicted values, and thin-skin data are illustrated in Figure 12. Although the Gardon gage data are consistently high, they are in reasonably good agreement with

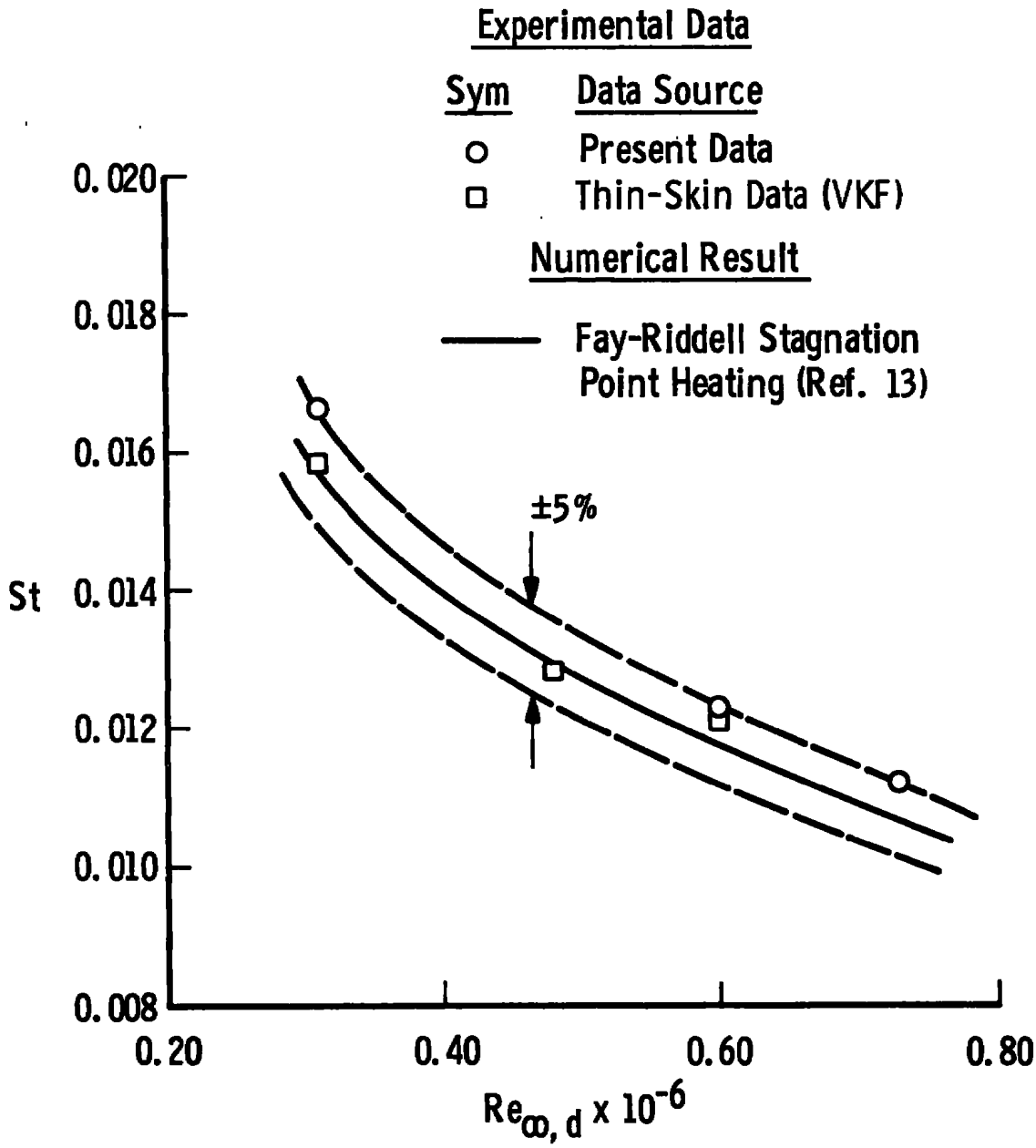

Figure 12. Comparison of theoretical and Gardon gage experimental stagnation point heat transfer.

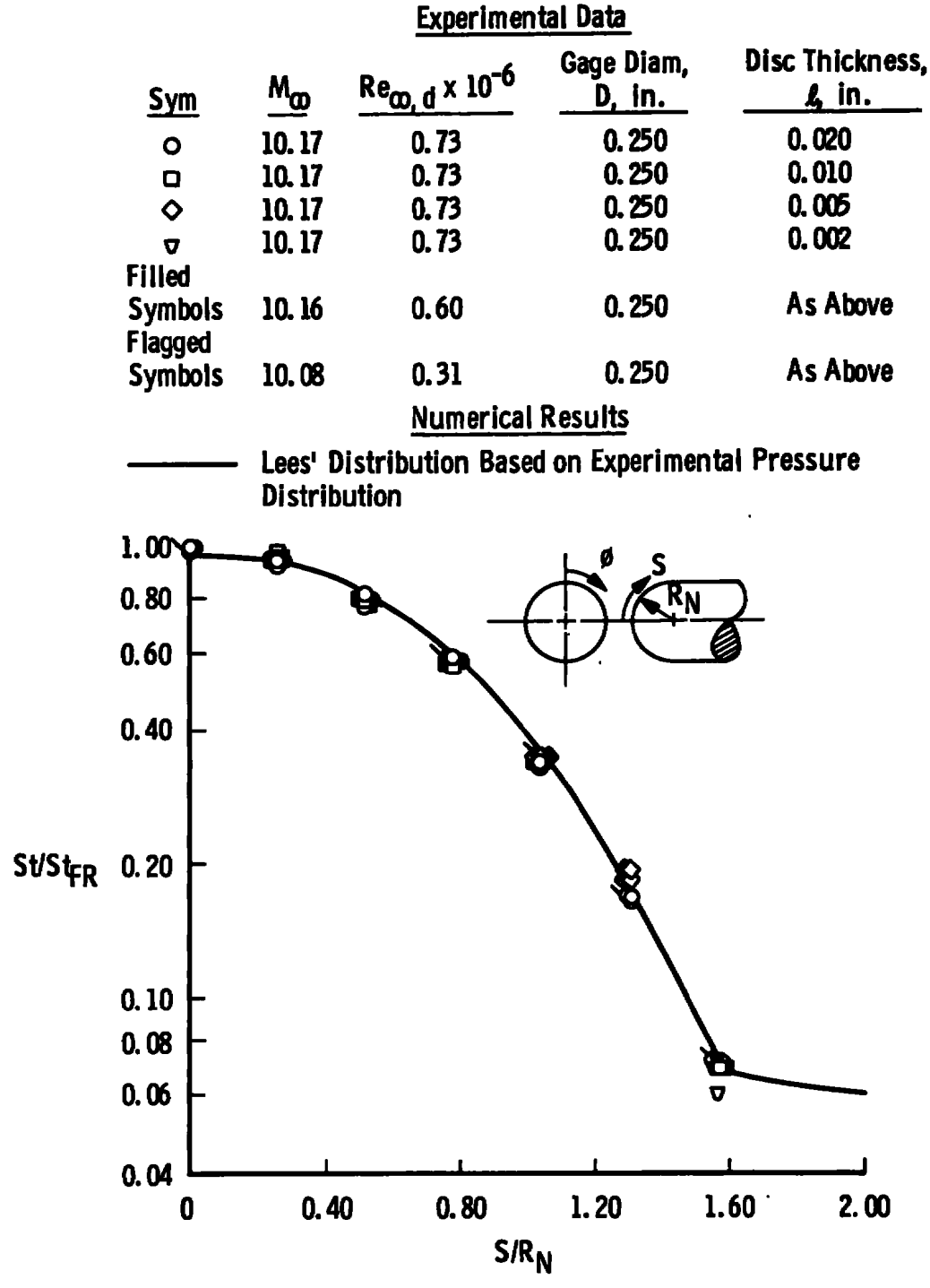

Figure 13. Effect of sensing disc thickness on Gardon gage indicated heat transfer, D = 0.250 inches.

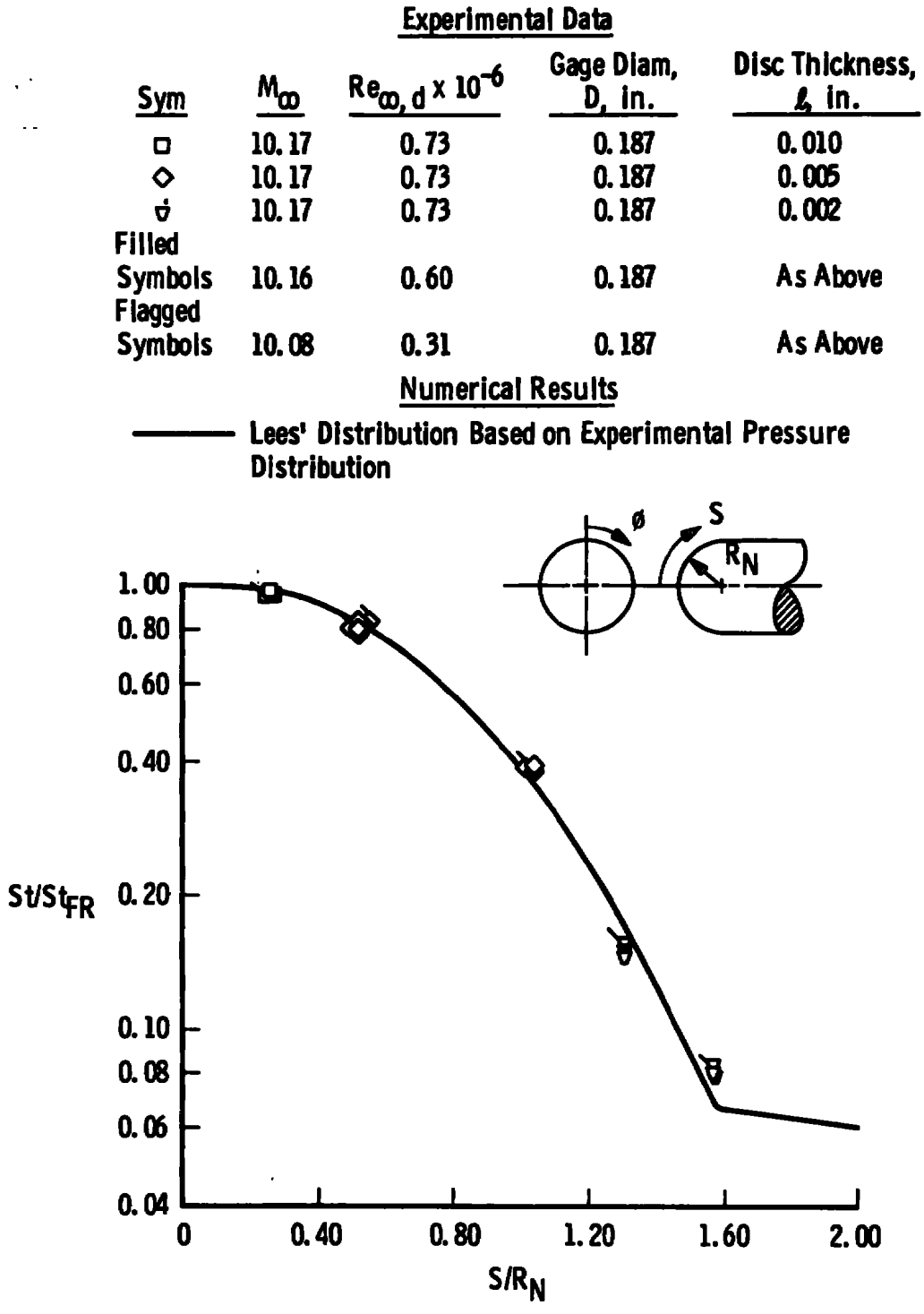

Figure 14. Effect of sensing disc thickness on Gardon gage indicated heat transfer, D = 0.187 inches.

Experimental Data

Sym	M_∞	$Re_{\infty,d} \times 10^{-6}$	Gage Diam, D, in.	Disc Thickness, ℓ, in.
◇	10.17	0.73	0.125	0.005
▽	10.17	0.73	0.125	0.002
Filled Symbols	10.16	0.60	0.125	As Above
Flagged Symbols	10.08	0.31	0.125	As Above

Numerical Results

——— Lees' Distribution Based on Experimental Pressure Distribution

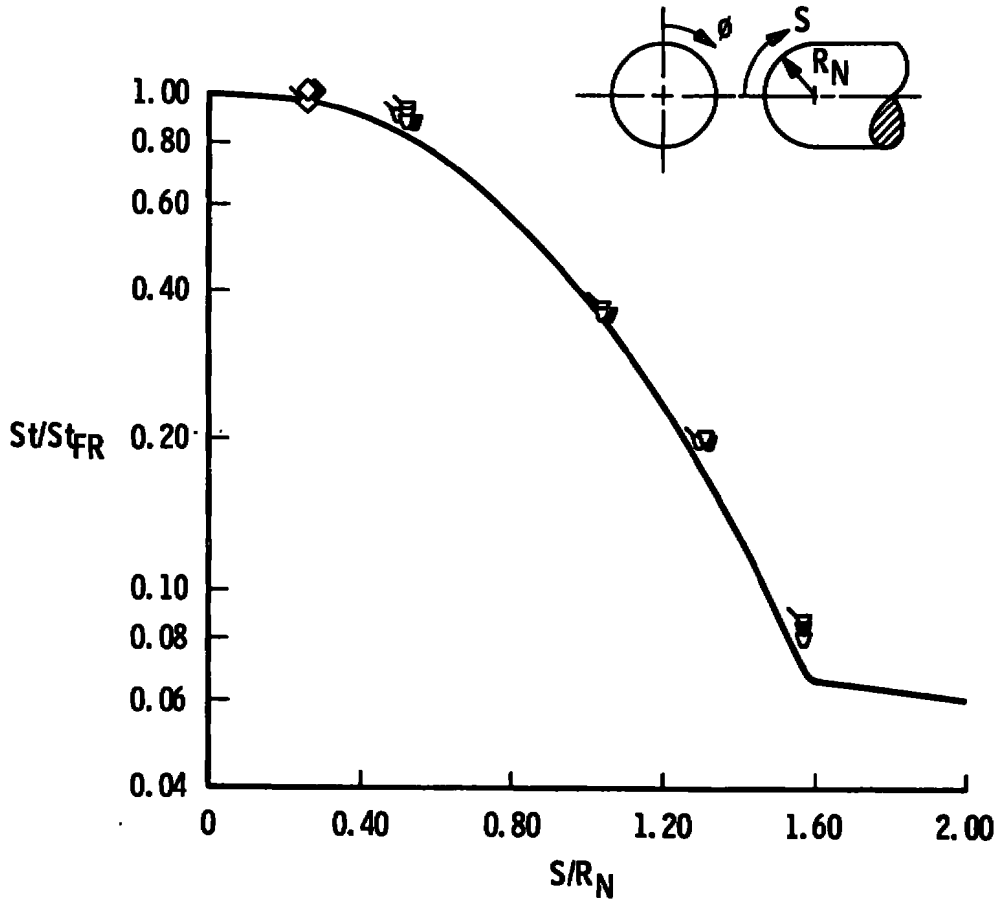

Figure 15. Effects of sensing disc thickness on Gardon gage indicated heat transfer, D = 0.125 inches.

Experimental Data

Sym	M_∞	$Re_{\infty,d} \times 10^{-6}$	d, in.	D, in.	Data Source
○	10.08-10.17	0.31-0.73	5.80	0.250	Average from
●	10.08-10.17	0.31-0.73	5.80	0.187	Figs. 13, 14,
◎	10.08-10.17	0.31-0.73	5.80	0.125	and 15
△	10.16	0.73	5.80	-	Thin-Skin Data (VKF)
○	8.69	0.94	3.00	-	Ref. 15
▫	8.01	1.68	5.80	-	Thin-Skin Data (VKF)

Numerical Results

—— Lees' Distribution Based on Experimental Pressure Distribution

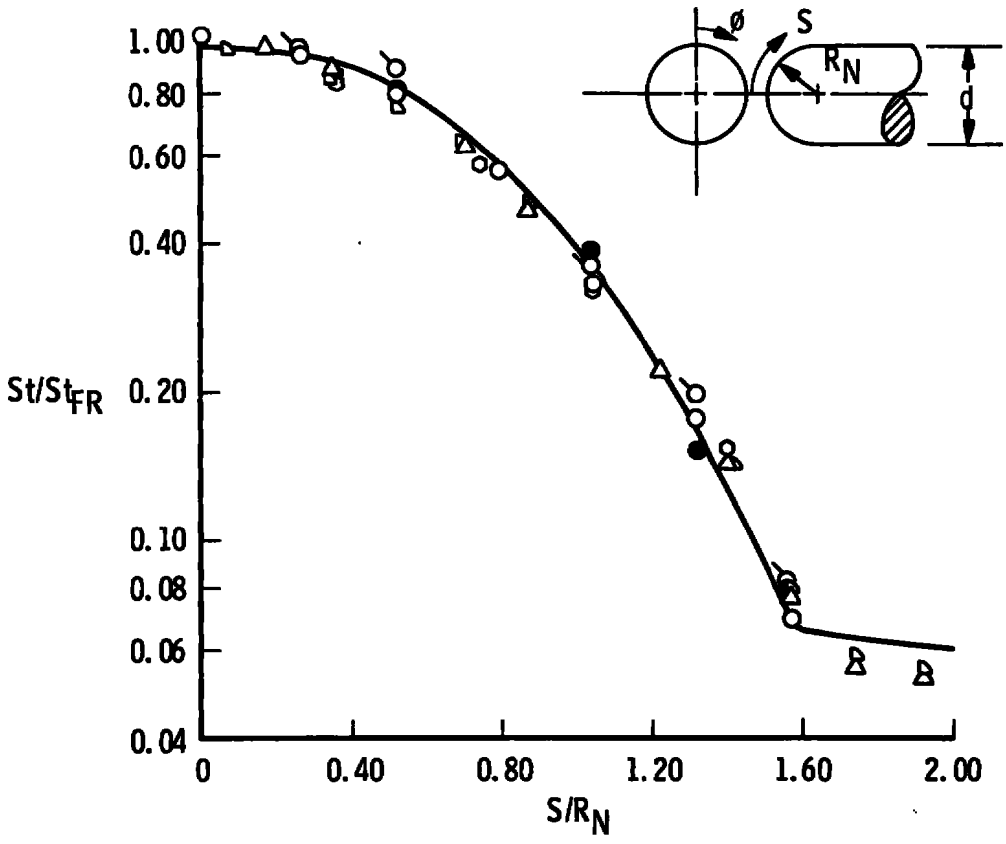

Figure 16. Summary comparison of Gardon gage data with theoretical and experimental heat transfer distributions.

both the theoretical values and the thin-skin data.

In Figure 13 the influence of sensing disc thickness on data from 0.25 inch diameter gages is illustrated. The data are in excellent agreement with Lees' distribution. Indeed, there appears to be no distinguishable trend with varying sensing disc thickness. Figures 14 and 15 show a similar lack of influence due to varying sensing disc thicknesses on data from 0.187 inch diameter and 0.125 inch diameter gages, respectively. However, there is increasing scatter in the data with decreasing gage diameter, particularly below $S/R_N \approx 1.20$. The gage sensitivity equation, Equation 16, shows that a gage sensitivity is more strongly influenced by gage radius changes than by variation in sensing disc thickness. Therefore, the 0.187 inch diameter and 0.125 inch diameter gages in the lower heating areas beyond $S/R_N \approx 1.20$ yielded electrical outputs below the lower limit stated in Table V, page 32.

A comparison of Gardon gage data with thin-skin data from two sources and with Lees' distribution is presented in Figure 16. The Gardon gage data illustrated in this figure were averaged according to diameter without regard for Reynolds number or sensing disc thickness. All of the Gardon gage data are in good agreement with both the theoretical and experimental distribution.

CHAPTER VI

CONCLUSIONS

Experimental convective heat transfer distributions on a hemisphere-cylinder model have been obtained using slug calorimeters and Gardon gages at a nominal Mach number of 10 over a Reynolds number range from 0.31×10^6 to 1.04×10^6 based on the model diameter (5.80 inches). Within the range of experimental conditions considered in this study, it may be concluded that Gardon gages can be employed to measure heat transfer distributions on blunt bodies at hypersonic Mach numbers. Indeed, the Gardon gage data were generally in good agreement with both theoretical predictions and thin-skin data.

Slug calorimeter data obtained in this study revealed several problems associated with using such devices in continuous flow wind tunnels. The most obvious problems noted were:

1. There is no clearly defined data reduction time for slug calorimeter data.
2. Conduction losses must be accounted for when analyzing slug calorimeter data.
3. Models instrumented with slug calorimeters probably will not yield satisfactory results when injected into the wind tunnel free-stream through the tunnel boundary layer.

Obviously, the instrumentation used in this investigation could be applied to aerodynamic shapes other than blunt bodies. However, the shape and depth of the instruments would have to be modified before they could be installed in slender bodies or thin wings and fins.

BIBLIOGRAPHY

BIBLIOGRAPHY

1. Ledford, R. L. "A Device for Measuring Heat Transfer Rates in Arc-Discharge Hypervelocity Wind Tunnels," Arnold Engineering Development Center TDR-62-64 (AD275740), Arnold Air Force Station, Tennessee, May, 1962.

2. Westkaemper, J. C. "An Analysis of Slug-Type Calorimeters for Measuring Heat Transfer from Exhaust Gases," Arnold Engineering Development Center TN-60-202 (AD245524), Arnold Air Force Station, Tennessee, November, 1960.

3. Conti, R. J. "Heat-Transfer Measurements at a Mach Number of 2 in the Turbulent Boundary Layer on a Flat Plate Having a Stepwise Temperature Distribution," National Aeronautics and Space Administration TND-159, Washington, D. C., November, 1959.

4. Rubesin, M. W. "The Effect of an Arbitrary Surface-Temperature Variation Along a Flat Plate on the Convective Heat Transfer in an Incompressible Turbulent Boundary Layer," National Advisory Committee for Aeronautics TN-2345, Washington, D. C., April, 1951.

5. Sivells, James C. "Aerodynamic Design and Calibration of the VKF 50-Inch Hypersonic Wind Tunnels," Arnold Engineering Development Center TDR-62-230 (AD299774), Arnold Air Force Station, Tennessee, March, 1963.

6. Howard, C. M. and H. T. Wood, Jr. "Mechanical Design of the 50-Inch Mach 10-12 Tunnel," Arnold Engineering Development Center TDR-62-229(AD402781), Arnold Air Force Station, Tennessee, April, 1963.

7. Gardon, Robert. "An Instrument for the Direct Measurement of Intense Thermal Radiation," The Review of Scientific Instruments, 24:366-370, May, 1953.

8. Kurzrock, John W. "Selection of Surface Thermometers for Measuring Heat Flux," Cornell Aeronautical Laboratory Report Number 124(AD404770), Cornell Aeronautical Laboratory, Incorporated, Buffalo 21, New York, February, 1963.

9. Ledford, R. L., W. E. Smotherman, and C. T. Kidd. "Recent Developments in Heat-Transfer-Rate, Pressure, and Force Measurements for Hotshot Tunnels," Arnold Engineering Development Center TR-66-228 (AD645764), Arnold Air Force Station, Tennessee, January, 1967.

10. Schneider, P. J. Conduction Heat Transfer. First edition. Reading, Massachusetts: Addison-Wesley Publishing Company, Incorporated, 1957.

11. Randall, R. E. "Thermodynamic Properties of Air: Tables and Graphs Derived from the Beattie-Bridgeman Equation of State Assuming Variable Specific Heats," Arnold Engineering Development Center TR-57-8 (AD135331), Arnold Air Force Station, Tennessee, August, 1957.

12. Morgan, Charles C. and Jack C. Andrews. "'Morgandyne' Heat-Transfer Transducer and a Flame-Torch Calibration Technique for Hypervelocity Wind Tunnels," Arnold Engineering Development Center TR-60-1 (AD232236), Arnold Air Force Station, Tennessee, February, 1960.

13. Fay, J. A. and F. R. Riddell. "Theory of Stagnation Point Heat Transfer in Dissociated Air," Journal of the Aeronautical Sciences, 25:73-85, February, 1958.

14. Lees, L. "Laminar Heat Transfer Over Blunt-Nosed Bodies at Hypersonic Flight Speeds," Jet Propulsion, 26:259-269, April, 1956.

15. Lauman, D. A. "Determining Aerodynamic Heating Rates Using Calorimetric Models in the Jet Propulsion Laboratory Hypersonic Wind Tunnel," Jet Propulsion Laboratory Memorandum Number 33-121, Pasadena, California, March, 1963.

16. Trimmer, Larry Lee. "A Study of the Blunt-Body Stagnation Point Velocity Gradient in Hypersonic Flow," Unpublished Master's thesis, The University of Tennessee, Knoxville, Tennessee, 1966.

17. Donovan, M. B. "A Survey of Stagnation Point Heating," The Boeing Company Report Number D2-22050 (AD444657), Seattle, Washington, January, 1963.

18. Cox, R. N. and L. F. Crabtree. Elements of Hypersonic Aerodynamics, New York: Academic Press, 1965.

APPENDIX

APPENDIX

HEAT TRANSFER THEORIES

Lees (14) formulated the following expression for the heat transfer rate at a distance S from the stagnation point of a blunt body:

$$\dot{q}(S) = 0.47\sqrt{(\rho_\delta \mu_\delta)_0 \, u_\infty} \, h_\delta \cdot F(S) \qquad \text{(A-1)}$$

The factor F(S) is a function of the body shape and flow conditions at the outer edge of the boundary layer and may be written as

$$F(S) = \frac{\dfrac{r_S}{\sqrt{2}} \left(\dfrac{P_\delta}{P'_0}\right) \left(\dfrac{\omega_\delta}{\omega_{\delta_0}}\right) \left(\dfrac{u_\delta}{u_\infty}\right)}{\left[\displaystyle\int_0^S \left(\frac{P_\delta}{P'_0}\right) \left(\frac{u_\delta}{u_\infty}\right) \left(\frac{\omega_\delta}{\omega_{\delta_0}}\right) r_S^2 \, dS \right]^{1/2}} \qquad \text{(A-2)}$$

where r_S is the cross-sectional body radius at the station of interest. Equation A-1 was derived within the limits of the following assumptions:

$$T_w << T_\delta$$

$$\rho_\delta \mu_\delta = \rho_w \mu_w$$

$$u^2/2 << h$$

$L = 1$

$P_r = 1$

At the stagnation point, S = 0, Equation A-1 becomes

$$\dot{q}_0 = 0.67\sqrt{(\rho_\delta \mu_\delta)_0}\, h_{\delta_0} \sqrt{\left(\frac{du_\delta}{ds}\right)_0} \qquad \text{(A-3)}$$

Assuming constant static pressure across the boundary layer, the quantity P_δ/P_0' becomes P_w/P_0' which was obtained from Trimmer's (16) experimental data. The velocity ratio, u_δ/u_∞, was computed from the following expression:

$$\frac{u_\delta}{u_\infty} = \frac{M_\delta \sqrt{T_\delta}}{M_\infty \sqrt{T_\infty}} \qquad \text{(A-4)}$$

The Mach number and temperature at the edge of the boundary layer were computed by assuming an isentropic expansion around the nose from a reservoir at the stagnation point as follows:

$$M_\delta = \left[\left(\left(\frac{P}{P_0'} \right)^{-\frac{\gamma - 1}{\gamma}} - 1 \right) \frac{2}{\gamma - 1} \right]^{1/2} \qquad \text{and}$$

$$T_\delta = T_0 \left(1 + \frac{\gamma - 1}{2} M_\delta^2\right)^{-1}$$

Hirshfelder's viscosity law was employed and is written as $\mu = (8.051 \times 10^{-10})T$.

The quantity ω is defined as

$$\omega = \frac{\mu}{RT}$$

The stagnation point velocity gradient, $(du_\delta/dS)_0$, was evaluated using the Newtonian approximation

$$\left(\frac{du_\delta}{dS}\right)_0 = \frac{1}{R_N}\sqrt{\frac{2(p_0 - p_\infty)}{\rho_0}} \qquad \text{(A-5)}$$

Assuming a perfect gas, all the individual elements are available to evaluate Equations A-1 and A-3. It appears that these two values are all that are necessary to make comparisons with experimental data. However, Donovan (17) and Cox and Crabtree (18) both point out that Lees' distribution and stagnation point value are generally as much as 20 per cent below experimental measurements.

A requirement still exists for a usable theoretical stagnation point heat transfer rate with which to nondimensionalize experimental data before making comparisons with Lees' distribution. Both References 17 and 18 state that Fay and Riddell's (13) stagnation point heat transfer formulation yields results which usually are in good agreement with experimental data. Their expression is

$$\dot{q}_0 = 0.94(h_0 - h_\delta)(\rho_w u_w)^{0.1}(\rho_\delta \mu_\delta)^{0.4}\sqrt{\left[\frac{du_\delta}{dS}\right]_0} \qquad \text{(A-6)}$$

The primary reason for the improved accuracy is that Fay and Riddell did not restrict the term $\rho\mu$ as Lees did. Reference 18 indicates that there is a factor $[\rho_w \mu_w/(\rho_\delta \mu_\delta)_0]^{0.1}$ for a Lewis number of unity between Equations A-3 and A-6 which may reach a value of 4 or 5 for a highly cooled surface. Additional assumptions used were:

$$Pr = 0.7$$

$$L = 1 \text{ and}$$

$$\mu = 2.27\frac{T^{3/2}}{T + 198.6} \times 10^{-8}$$

Additional terms already discussed are available for numerical evaluation of Equation A-6.

UNCLASSIFIED
Security Classification

DOCUMENT CONTROL DATA - R & D

(Security classification of title, body of abstract and indexing annotation must be entered when the overall report is classified)

1. ORIGINATING ACTIVITY (Corporate author)	2a. REPORT SECURITY CLASSIFICATION
Arnold Engineering Development Center ARO, Inc., Operating Contractor Arnold Air Force Station, Tennessee	UNCLASSIFIED
	2b. GROUP N/A

3. REPORT TITLE

AN EXPERIMENTAL METHOD FOR DETERMINING HEAT TRANSFER DISTRIBUTIONS ON BLUNT BODIES AT HYPERSONIC MACH NUMBERS

4. DESCRIPTIVE NOTES (Type of report and inclusive dates)

December 1966 to January 1968 - Final Report

5. AUTHOR(S) (First name, middle initial, last name)

Frederick K. Hube, ARO, Inc.

6. REPORT DATE	7a. TOTAL NO. OF PAGES	7b. NO. OF REFS
June 1969	68	22

8a. CONTRACT OR GRANT NO.	9a. ORIGINATOR'S REPORT NUMBER(S)
F40600-69-C-0001 b. PROJECT NO. 876A c. Program Element 65401F d.	AEDC-TR-69-20
	9b. OTHER REPORT NO(S) (Any other numbers that may be assigned this report) N/A

10. DISTRIBUTION STATEMENT

This document has been approved for public release and sale; its distribution is unlimited.

11. SUPPLEMENTARY NOTES	12. SPONSORING MILITARY ACTIVITY
Available in DDC	Arnold Engineering Development Center, Air Force Systems Command, Arnold AF Station, Tennessee 37389

13. ABSTRACT

Experimental convective heat transfer distributions on a hemisphere-cylinder configuration were obtained using slug calorimeters and Gardon gages. Wind tunnel tests were conducted at a nominal Mach number of 10 over a free-stream Reynolds number range from 0.31×10^6 to 1.04×10^6 based on the model diameter (5.80 inches). The data were compared with theoretical heat transfer values and data obtained with thin-skin calorimetric wind tunnel models. The slug calorimeter data were highly time dependent due to conduction heat losses; consequently, the data did not compare favorably with theoretical predictions. Gardon gage indicated heat transfer was in very good agreement with both theoretical values and data from other sources.

DD FORM 1 NOV 65 1473

UNCLASSIFIED
Security Classification

14. KEY WORDS	LINK A ROLE	LINK A WT	LINK B ROLE	LINK B WT	LINK C ROLE	LINK C WT
blunt bodies						
heat transfer						
wind tunnel tests						
hypersonic flow						
calorimeters						
measuring instruments						

1. Blunt nosed bodies -- Heat transfer
2. " " " -- Hypersonic flow
3. Heat transfer -- Measurements
4. Calorimeters

15-7